frontiers | Frontiers in Marine Science

TYPE Original Research
PUBLISHED 20 December 2024
DOI 10.3389/fmars.2024.1515112

OPEN ACCESS

EDITED BY
Ivana Veneza,
Federal University of Western Pará, Brazil

REVIEWED BY
Amit Ranjan,
Tamil Nadu Fisheries University, India
Sanal Ebeneezar,
Central Marine Fisheries Research Institute (ICAR), India

*CORRESPONDENCE
Tongjun Ren
tongjunren@dlou.edu.cn

†These authors share first authorship

RECEIVED 22 October 2024
ACCEPTED 06 December 2024
PUBLISHED 20 December 2024

CITATION
Chen Y, Zhang Y, Zhang R, Deng H, Meng X, Inaba K, Osato T, Zhao X, Han Y and Ren T (2024) Adaptive mechanisms to hypoxia and hyperoxia in juvenile turbot, *Scophthalmus maximus*. *Front. Mar. Sci.* 11:1515112. doi: 10.3389/fmars.2024.1515112

Adaptive mechanisms to hypoxia and hyperoxia in juvenile turbot, *Scophthalmus maximus*

Yi Chen[1†], Yuntian Zhang[1†], Rongwei Zhang[1], Hongsheng Deng[1], Xiangyu Meng[1], Kotoya Inaba[2], Tatsu Osato[2], Xiaoran Zhao[1,3], Yuzhe Han[1,3] and Tongjun Ren[1,3*]

[1]College of Fisheries and Life Science, Dalian Ocean University, Dalian, Liaoning, China, [2]Industry gas devision, Iwatani Co., Ltd., Japan, Tokyo, Japan, [3]Dalian Key Laboratory of Breeding, Reproduction and Aquaculture of Crustaceans, Dalian Ocean University, Dalian, Liaoning, China

In recirculating aquaculture systems (RAS), the impact of dissolved oxygen (DO) fluctuations on turbot is still not fully understood. This study investigated these impacts by selecting 135 turbot (average dry weight: 6.0 ± 0.5 g) and exposing them to three DO levels: hypoxia (4.0 ± 0.5 mg/L), normoxia (7.5 ± 0.5 mg/L), and hyperoxia (23.5 ± 0.5 mg/L). These groups were labeled as LF (low oxygen), NF (normal oxygen), and HF (high oxygen). The study aimed to explore the adaptive mechanisms of turbot under hypoxic and hyperoxic conditions, using microbiome, transcriptome, and hematological analyses over a 40-day period. The results suggest that hyperoxia significantly enhances turbot growth without compromising the composition of intestinal microbiome, whereas hypoxia markedly impairs growth and induces alterations in intestinal microbiome. Transcriptomic analysis revealed various pathways implicated in adaptation to both hypoxic and hyperoxic conditions, encompassing amino acid metabolism, protein metabolism, lipid metabolism, carbohydrate metabolism, the PPAR signaling pathway, etc. However, pathway changes are not completely consistent. For instance, pancreatic secretion is crucial for hyperoxia adaptation, while the HIF1α pathway plays a key role in hypoxia adaptation and tissue repair. Furthermore, genes *ATP6*, *HIF1*, *HSP90*, and *CYP450* exhibited high expression levels during hypoxia, whereas *Hbae5* and *Man-SL* showed elevated expression during hyperoxia. In hematological indicators, there are ways to help adapt to hypoxia and hyperoxia, including increased red blood cell (RBC) and hemoglobin (HGB) counts; gas and ion balance; elevated blood urea nitrogen (BUN) and malondialdehyde (MDA); increased polyphenol oxidase (PPO) and lysozyme (LZM) activity. Although turbot have adaptive mechanisms to both hypoxia and hyperoxia, extended exposure to hypoxia detrimentally affects growth, whereas hyperoxia facilitates it. These findings provide significant insights into the adaptive mechanisms of turbot in response to fluctuating DO levels.

KEYWORDS

***Scophthalmus maximus*, hypoxia, hyperoxia, oxygen nanobubbles, RAS**

1 Introduction

Over the past two decades, the aquaculture industry has made significant progress. However, it has encountered bottlenecks, including but not limited to conflicts with sustainable development and environmental protection (Naylor et al., 2021), as well as substantial losses caused by fluctuations in dissolved oxygen (DO) levels (Yaparatne et al., 2024). High-density recirculating aquaculture systems (RAS) offer multiple benefits, including reduced climate dependence, lower environmental pollution, decreased water usage, and improved land-use efficiency (Ahmed and Turchini, 2021; Engle, 2023). Despite these advantages, RAS has not fully replaced traditional aquaculture models due to challenges like high energy consumption, elevated costs, and hypoxic risks from high-density stocking or power outages (Badiola et al., 2018). DO levels are critical for the survival of aquatic animals (Chen et al., 2025); very low levels (DO < 4 mg/L), classified as hypoxia, can be lethal to fish (Rector et al., 2022). Both air aeration technology and nanobubble oxygen (NB-O_2) technology can improve DO levels; however, NB-O_2 technology offers more distinct advantages, such as reduced electricity costs, better DO regulation, and the creation of hyperoxic conditions to accommodate high-density aquaculture, among others (Yaparatne et al., 2024). These benefits have been demonstrated in fish production. For example, NB-O_2 has been shown to promote the growth of rainbow trout (*Oncorhynchus mykiss*), grouper (*Epinephelus* sp.), and Nile tilapia (*Oreochromis niloticus*) (Ebina et al., 2013; Hanif et al., 2021; Linh et al., 2023). Additionally, when used as a carrier for chitosan, NB-O_2 has emerged as a novel vaccine strategy for preventing *Vibrio harveyi* infections in Asian seabass (*Lates calcarifer*) (Thu Lan et al., 2024). This technology not only improves fish survival rates but also reduces energy costs associated with aeration, positioning NB-O_2 as an innovative solution within RAS.

Nanobubbles are bubbles with a diameter smaller than 200 nm (Agarwal et al., 2011). Nanobubbles can be classified based on the gas they contain, such as NB-O_2, NB-O_3, NB-CO_2, NB-H_2, and NB-N_2, among others (Yaparatne et al., 2024). Nanobubble technology has applications across various fields, including water treatment (Nguyen et al., 2024), agriculture (Zhou et al., 2022), and aquaculture. In this aquaculture research, NB-O_2 was produced using a nanobubble generator with liquid oxygen as the reservoir. As oxygen moved through an insulated pipe into Venturi tubes, it followed a threaded path, dispersed, and entered the pump's high-pressure outlet, forming NB-O_2 (Foudas et al., 2023). Due to its neutral buoyancy, NB-O_2 can remain suspended in liquids for several weeks, accumulating to improve gas solubility and utilization (Soyluoglu et al., 2021). So much as, it can enhance the DO level to reach 25 mg/L or higher, a condition referred to as hyperoxia (Nghia et al., 2022).

The turbot, *Scophthalmus maximus*, is a cold-water marine fish, known for its disc-shaped body, bottom-dwelling behavior, and carnivorous diet (Bao, 2022). Due to its rapid growth, high-quality fillets, and significant commercial value, turbot has become an important farmed species in Europe and East Asia, with annual production in China reaching about 50,000 tons (Qiao et al., 2019; Chen et al., 2025). Previous research has examined turbot's response to different DO levels. At DO levels of 2–4 mg/L, turbot displayed poor growth, reduced feeding, impaired swimming, and metabolic issues (Pichavant et al., 2002; Ma et al., 2024). When treated with hyperoxia (DO 11–14 mg/L) for 42 days, turbot with an initial dry weight of 16 grams experienced gill damage and reduced growth (Wu et al., 2016), which contrasts with the reported positive effects of hyperoxia in NB-O_2 technology. Although NB-O_2 technology has shown benefits in aquaculture, there is limited research on how turbot adapts to hyperoxia using omics approaches, and no studies specifically address the application of NB-O_2 in turbot farming. Therefore, we use an omics approach that provides a comprehensive view of microbial and genetic responses to DO, offering insights beyond conventional physiological measures.

This study aims to investigate the adaptive mechanisms of Scophthalmus maximus to NB-O_2-induced hypoxia and hyperoxia by examining the microbiome, transcriptome, and hematological responses.

2 Methods

2.1 Fish and materials

Juvenile turbots, with an average dry weight of 6.0 ± 0.5 g, were sourced from Dalian Tianzheng Industrial Co., Ltd., China. The fish displayed consistent size, no visible injuries, and heath. The health standards for the turbots are as follows: normal external appearance, including the absence of lesions on the gills, mouth, and tail; normal behavior, including no avoiding shoal of fish, no backstroke, no lateral lying, and no hunger strike. They were then transferred to the Aquarium Laboratory at Dalian Ocean University (38°52'2" N, 121°32'56" E) for experimentation. Feed was provided by Dalian Shengtai Biotechnology Co., Ltd., China. A nanobubble generator and a 300-liter liquid oxygen gas tank were supplied by the Industry Gas Division of Iwatani Co., Ltd., Japan.

2.2 Design and management

Three groups (LF, NF, HF) were tested in separate recirculating aquaculture systems (RAS), with all conditions kept consistent except for the dissolved oxygen (DO) levels, which served as the experimental variable. DO levels were set to replicate hypoxic (LF), normoxic (NF), and hyperoxic (HF) conditions, relevant for optimizing RAS environments. Previous research indicates that turbot can normal survive and grow, under both long-term hypoxia at DO levels of 3–5 mg/L and normoxia at 7–8 mg/L (Wu et al., 2016). Additionally, after 42 days of exposure to hyperoxic conditions (DO 23–24 mg/L) using NB-O_2 technology, Nile tilapia showed normal growth (Linh et al., 2023), which established the hyperoxia benchmark for this study. In the LF group, DO was maintained at 4.0 ± 0.5 mg/L by pure nitrogen. The NF group used an aeration pump to keep DO at 7.5 ± 0.5 mg/L by air, while the HF group achieved a DO

level of 23.5 ± 0.5 mg/L by pure liquid oxygen through a Venturi tube into NB-O_2. DO levels were continuously monitored with a fluorescence DO meter (YUDADA, Jiangsu Yuyuyu Technology Co., Ltd., China).

After a one-week acclimation period, turbot were randomly assigned to individual 100 L tanks, with three replicate tanks per group, each containing 15 fish. Each tank in the RAS had independent water inlets and outlets. Sewage treatment involved consistent filtration, sterilization, and ammonia removal. For 40 days, the fish were fed twice daily at 10:00 and 17:00, with the feed amount set at 4% of their body weight. Tanks were illuminated by an aquarium lamp for 12 hours each day to facilitate feeding, and weekly adjustments to the feed quantity were made as necessary (Wu et al., 2024). Uneaten feed and feces were removed daily, and a 5% water change was performed, with one-third of the total tank volume replaced every 10 days. The experiment was carried out under stable conditions, with water quality indicators checked every two days. The indicators were as follows: pH maintained at 8.5 ± 0.1, salinity at 30 ± 0.5 ‰, and temperature at 16 ± 0.5°C. Other indicators remained normal and constant throughout the study.

2.3 Sample collection

Feeding was stopped 24 hours prior to sample collection. Turbots were anesthetized using an eugenol (40 ± 5 mg/L, 15 ± 1°C) water bath and dissected on ice. The fish's body surface was disinfected with 75% alcohol, and seawater was removed using gauze. Body weight, body length, and visceral weight were recorded. Blood samples were drawn from the tail vein using a sterile 1 mL syringe, with heparin sodium (5 mg/mL, physiological saline solution) added as an anticoagulant at a ratio of 1:5. The blood was transferred into sterile frozen tubes and transported to an animal hospital for routine and gas analyses on the same day. The remaining blood was centrifuged at 3000 rpm (RCF: 1000 g) for 10 minutes using a centrifuge (TGL-16G-A, Shanghai Anting Scientific Instrument Factory, China), and the supernatant was stored at −20°C for enzyme activity and biochemical analyses. Gill and intestine samples were collected in sterile cryopreservation tubes, frozen in liquid nitrogen, and stored in an ultra-low temperature freezer at −80°C for further analysis.

2.4 Growth equations

Growth performance was calculated using methods from Li and Wang (Li et al., 2019; Wang et al., 2024). Body indices were measured at baseline and post-treatment. The following abbreviations are used for body indicators and growth performance: IBL, initial body length; FBL, final body length; IBW, initial body weight; FBW, final body weight; VSI, visceral index; ISI, intestinal index; LVI, liver index; BWG, body weight gain; FCR, feed conversion rate; SR, survival rate; SGR, specific growth rate; RR, respiratory rate; and CF, coefficient of fatness. The formulas for these measurements are as follows:

$$\mathrm{VSI}(\%) = [\text{Visceral weight(g)}/\text{Body weight(g)}] \times 100,$$

$$\mathrm{ISI}(\%) = [\text{Intestinal weight(g)}/\text{Body weight(g)}] \times 100,$$

$$\mathrm{LVI}(\%) = [\text{Liver weight(g)}/\text{Body weight(g)}] \times 100,$$

$$\mathrm{BWG}(\%) = [\mathrm{FBW(g)} - \mathrm{IBW(g)}]/\mathrm{IBW(g)} \times 100,$$

$$\mathrm{FCR}(\%) = \text{Feed consumed(g)}/[\mathrm{FBW(g)} - \mathrm{IBW(g)}] \times 100,$$

$$\mathrm{SR}(\%) = (\text{Final fish number}/\text{Initial fish number}) \times 100,$$

$$\mathrm{SGR}(\%/\mathrm{day}) = [\ln \mathrm{FBW(g)} - \ln \mathrm{IBW(g)}]/\mathrm{days} \times 100,$$

$$\mathrm{RR(n/min)} = \text{Respiratory numbers(n)}/\text{Times(min)},$$

$\mathrm{CF}(g/cm^3) = [\mathrm{FBW}(g)/\mathrm{FBL}^3(cm^3)] \times 100$, CF is defined as the weight of fish meat (in grams) per cubic centimeter of volume.

2.5 Microbiome sequencing

After a 24-hour fasting period, three healthy turbots were randomly selected from each group and disinfected with 70% ethanol. Intestinal tissue and contents were aseptically collected from the dissected fish. The samples were sent to Shanghai Majorbio Bio-Pharm Technology Co., Ltd. (China) for microbiome sequencing. The V3–V4 region of the bacterial 16S rRNA gene was PCR amplified using universal primers 338F-5'ACTCCTACGGGAGGCAGCAG3' and 806R-5'GGACTACHVGGGTWTCTAAT3' (Chen et al., 2024). Following DNA extraction, concentration was verified via electrophoresis on a 1% agarose gel, and PCR amplification was performed using TransGen AP221-02. The PCR products were quantified using the QuantiFluor™-ST Blue fluorescent quantitation system (Promega), with electrophoresis results serving as a reference for concentration measurements. Samples were then proportionally mixed for Illumina library construction and sequencing (Schurch et al., 2014). Operational taxonomic unit (OTU) clustering was conducted using Uparse 11, with non-redundant sequences (excluding singletons) clustered at 97% similarity. During the clustering process, chimeric sequences were removed, and representative sequences for each OTU were obtained (Tan et al., 2022). The classification of these representative sequences was then carried out using the Bayesian algorithm of the RDP classifier (Guo et al., 2024). PICRUSt 2 was used to predict KEGG functions at the third level of the microbiome. This methodology is based on the work of Guo et al (Wang, 2022), and the data are stored in the Sequence Read Archive (SRA) of the NCBI database under accession number PRJNA1159012.

2.6 Transcriptome sequencing

Building on the detailed transcriptome analysis of turbot under hypoxia by Wang Q (Guo et al., 2024), this study focuses exclusively on transcriptome data under hyperoxia. This study followed the

guidelines of Schurch et al. (Schurch et al., 2016) for transcriptome sequencing with biological replicates not less than 6. Nine biological replicates were constructed for each group, with the specific procedure as follows: 18 fish from 6 tanks (three replicates per group, i.e., three tanks each for NF and HF groups) were used to create 6 samples. Each sample consisted of gills from 3 fish, which were then flash frozen in liquid nitrogen and stored at −80°C. Transcriptome sequencing was then performed on these six samples. Total RNA was extracted using QIAzol Lysis Reagent (Qiagen, Germany) and purified with the RNA Purification Kit (Majorbio, China). RNA concentration was verified using an agarose gel (Biowest, Spain). Following RNA quantification, mRNA levels were assessed, and cDNA was synthesized, followed by adapter ligation and PCR amplification. Illumina libraries were constructed, and high-throughput sequencing was performed on the NovaSeq X Plus platform, Shanghai Majorbio Biomedical Technology Co., Ltd., China.

For data processing, calculate Q20, Q30, and QC ratios for sequencing data quality assessment, and then Fastp was used to filter the raw reads and assess sequencing quality (Chen, 2023). According to the method provided by Mortazavi et al (Mortazavi et al., 2008), HiSat2 was employed to align the filtered results with the turbot reference genome (NCBI ID GCF_022379125.1). Gene expression levels were analyzed using RSEM. Differentially expressed genes (DEGs) were identified using DEGseq (Liu et al., 2024), based on the criteria of FDR < 0.05 & $|\log_2 FC| \geqq 1$ (Anders and Huber, 2010). Gene functions were annotated using the Gene Ontology (GO datebase) and Kyoto Encyclopedia of Genes and Genomes (KEGG datebase) (Hays et al., 2023). Enrichment analysis was performed with a padjust < 0.05 considered significant, with GO enrichment conducted using Goatools and KEGG enrichment analyzed using Python scipy (Miranda et al., 2024). The transcriptome data are stored in the SRA of the NCBI GeneBank database under accession number PRJNA1118073.

2.7 Real-time quantitative PCR

To validate the transcriptome sequencing results for genes related to DO levels, RT-qPCR was conducted on 18 target genes. Genes and primers sequences are listed in Table 1. Numbers 1-10 are the top 10 DEGs from the transcriptome data under hyperoxia, selected based on the criteria of FDR < 0.05 & $|\log_2 FC| \geqq 2$, arranged in descending order of $|\log_2 FC|$, and are included for validation purposes. Numbers 11–18 are target genes associated with DO, which not only validate the high-oxygen transcriptome data but also provide insights into their expression profiles under both hypoxic and hyperoxic conditions. Number 19 (β-actin) is the internal reference gene. In detail, five gill samples from each group were collected, and total RNA was extracted using the RNA Easy Fast kit (TIANGEN, Beijing, China). RNA concentrations were adjusted to 1000 ng/μL, followed by reverse transcription to cDNA using the FastKing gDNA Dispersing RT SuperMix (TIANGEN, Beijing, China). Primers were designed with Premier 5.0 and synthesized by Sangon Biotechnology Co., Ltd., China. The newly designed primers were primarily validated for specificity and sensitivity through PCR (Lee et al., 2010). The validation process involved using a minimal amount of cDNA (10–20 ng) in the PCR experiment to test sensitivity, with normal amplification confirming sensitivity. A negative control group (without cDNA) was included to ensure non-pollution; in the positive group (add cDNA), the melting curves were generated to ensure the specificity of amplified products at the end of PCR. The amplification efficiency of primers was between 90 and 110%, and the correlation coefficient was over 0.9 for each gene (Ma et al., 2024). The β-actin gene served as the internal control for RT-qPCR analysis. RT-qPCR was performed using the SYBR Green I dye method, with the SGExcel FastSYBR qPCR Premix kit (Sangon, Shanghai, China). The total reaction volume was 20 μL, comprising 10 μL SYBR Green I, 8.2 μL ddH_2O, 1 μL cDNA, and 0.8 μL of both forward and reverse primers. Each sample was analyzed in triplicate using the Roche LightCycle 480 real-time PCR system (Roche Basel SH) under the following cycling conditions: 95°C for 3 min (polymerase activation), followed by 40 cycles of 95°C for 5 s, 60°C for 20 s, 95°C for 15 s, 60°C for 1 min, 95°C for 15 s, and 60°C for 15 s. The complete operation process of RT-qPCR refers to Zhang (Zhang et al., 2024). Data were analyzed using the $2^{-\Delta\Delta CT}$ method (Livak and Schmittgen, 2001), with the NF group as the control.

2.8 Hematological testing

Whole blood samples were collected in frozen tubes, stored in ice, and sent to veterinary hospitals for two types of analysis, routine tests, and gas pressures and ion balances. Blood from five fish was pooled into a single frozen tube as a repetition, with three replicates for each group. Blood routine tests were assessed using an automatic blood cell analyzer (BC-5000Vet, Shenzhen Mindray Animal Medical Technology Co., Ltd., China). Blood routine parameters include: WBC, white blood cells; RBC, red blood cells; HGB, hemoglobin; TP, total protein; ALB, albumin; GLOB, globulin; HCT, hematocrit; MCV, mean corpuscular volume; and PLT, platelets. Blood gas pressures and ion balances were measured using a blood gas analyzer (Radiometer ABL9-2, Shanghai Redumit Medical Equipment Co., Ltd., China). Blood gas and ion balance parameters including: C(tO2e), total oxygen concentration; $S(O_2)$, oxygen saturation. Among the remaining indicators, P represents gas partial pressure, $P(O_2)$, $P(CO_2)$; and C represents concentration, $C(CO_2)$, $C(HCO_3^-)$, $C(Cl^-)$, $C(H^+)$, $C(Na^+)$, (K^+), and $C(Ca^{2+})$.

Blood metabolic indicators and enzyme activities were measured using blood plasma, introduced in order of name, identification number, and wavelength. Metabolic indicators include: CHO, cholesterol, A111-1-1, 500 nm; TG, triglycerides, A110-2-1, 500 nm; GLU, glucose, A154-1-1, 505 nm; BUN, blood urea nitrogen, C013-1-1, 520 nm; CRE, creatinine, C011-2-1, 546 nm; and MDA, malondialdehyde, A003-1-1, 532 nm. Enzyme activities include: ACP, acid phosphatase, A060-2-1, 520 nm; AKP, alkaline phosphatase, A059-2, 520 nm; LDH, lactate dehydrogenase, A020-1, 440 nm; SDH, succinate dehydrogenase, A022-1-1, 600 nm; GPT, glutamic pyruvic transaminase, C009-2-1, 505 nm; GOT, glutamic oxalacetic transaminase, C010-2-1, 505 nm; PPO, polyphenol oxidase, A136-1-1, 420 nm; LZM: lysozyme, A050-1-1, 530 nm. The determination of metabolic indicators and enzyme activities was performed using spectrophotometry following the manufacturer's

TABLE 1 RT-qPCR primer design table.

Number	Target gene	Gene ID	Forward primer sequence (5′ to 3′)	Reverse primer sequence (5′ to 3′)	ProdSize
1	*LOC5547*	LOC118285547	TGTTTGAGGACCCAGCACCATTTG	CCTGACTTGTGGCGAGCAACC	115
2	*TG1*	LOC118284830	TGGAGGAGGTGGTCAGCAGTTG	GAGCAGCAGCATCGTGAAGAGG	95
3	*IIP44*	LOC118302793	GCCTCTCACTCAACCGCATCTTTC	AGAATCGGAGCGTCAATGGCATC	82
4	*EPOD*	LOC118313990	AGCAATGTCCGTCAGCAGATGAAC	GCCGTTGTCAGTGTACCGTGTG	150
5	*GTP7*	LOC118314837	GGAAGCCACTACACCAACGAGATG	TCCTCCCTCTCTTTGCGTATCTGC	110
6	*MYH1s*	LOC118315112	CAAGCAGAAGCAGCGTGAGGAG	GAGCCTTCAGCATGTCAGCAGAG	104
7	*PA2LY6*	LOC118318819	GCTCGGGACAACTACCTTTCTTCG	CAGGTGTCACTGGCAGCAGATG	121
8	*Mucin5*	LOC124850859	TGCTCCGACAACAACAACTCCTG	TCATCGTTGAAGTGGCTGCTGTAG	101
9	*FNDC7*	LOC118311675	GTCCGCAACTACACCACCATTCC	TTAGTCTCCTCTGCTGTCGTCTCG	134
10	*NOS1*	LOC118314181	AACCTGTCCTCTCCGTCCATCAC	CCTTCAGCAGCTCGTTGTTCTCC	139
11	*ATP6*	8382077	TTGCTCGGTATTCCCTTAATTGCTC	TCTGAAATGATAAGAGTCGGTTGGC	115
12	*ATP8*	8382076	TGCCCGCCCCGTGATTTG	CTTTGAGAAGTAGGGGTATTCGGATAC	109
13	*COX1*	8382074	ATGGGAATAGTGTGAGCGATAATAGC	CATTGTAGCGGAGGTGAAGTAAGC	120
14	*HIF1*	LOC118286010	GACTACTACCGGGCACAAGG	CTCAATGTTGGAGGGGTGCT	82
15	*Hbae5*	LOC118287911	TGAAGGAGCACGGAAGGAAGG	GTGGGACAGGAGCTTGAAGTTG	146
16	*Man-SL*	LOC118317069	CCTTCTGCAACCGGATAACAACC	AAGAACCAGCCGACCTCCATC	133
17	*HSP90*	LOC118315542	ATCGCAGAGGAACACTACAATGATAAG	TGTCACTGTTGGAGGTCTGGAAG	133
18	*CYP450*	LOC118284036	GGCAACAGGCAGCGACACAG	CTCCAGCAATGGCATCCACACC	80
19	*β-actin*	LOC118288414	TCGTGCTGTCTTCCCTTCTATCG	TGCTCTGGGCTTCATCACCTAC	101

Numbers 1 – 10 are the 10 differentially expressed genes (DEGs) selected with FDR < 0.05 and the highest fold changes in NF vs HF. Numbers 11 – 18 are 8 selected target genes related to dissolved oxygen adaptation, and number 19 is an internal reference gene. Genes description: *LOC5547*, uncharacterized LOC118285547; *TG1*, thyroglobulin, transcript variant X1; *IIP44*, interferon-induced protein 44-like; *EPOD*, eosinophil peroxidase-like; *GTP7*, GTPase IMAP family member 7-like; *MYH1s*, myosin heavy chain, fast skeletal muscle, transcript variant X1; *PA2LY6*, phospholipase A2 inhibitor and Ly6_PLAUR domain-containing protein; *Mucin5*, mucin-5AC-like; *FNDC7*, fibronectin type III domain containing 7a; *NOS1*, nitric oxide synthase 1 (neuronal); *ATP6*, ATP synthase F0 subunit 6; *ATP8*, ATP synthase F0 subunit 8; *COX1*, cytochrome c oxidase subunit I; *HIF1*, hypoxia inducible factor 1 subunit alpha, like, transcript variant X1; *Hbae5*, hemoglobin, alpha embryonic 5; *Man-SL*, mannose-specific lectin-like; *HSP90*, heat shock protein 90, beta (grp94), member 1; *CYP450*, cytochrome P450, family 1, subfamily B, polypeptide 1; *β-actin*, actin, beta 2. *β-actin* is an internal reference gene.

instructions. All test kits were sourced from Nanjing Jiancheng Institute, China. The equipment used was a light absorption microplate reader (ReadMax 500F, Shanghai Shining Biotechnology Co., Ltd., China).

2.9 Statistical analysis

Data were analyzed using IBM SPSS 27, presenting results as mean ± standard deviation (SD). Due to the large sample size in each group, the average value from five individual turbots was used for each of the three replicates (n = 3). The Shapiro-Wilk test was used to analyze whether the data follow a normal distribution. If the data are normally distributed ($P > 0.05$), a one-way ANOVA was performed directly. If the data are not normally distributed ($P < 0.05$), logarithmic transformation (base 10) was applied to reduce the variance disparity before performing one-way ANOVA. One-way ANOVA was employed to assess differences between groups, with *post-hoc* tests conducted using Tukey and Duncan methods. $P < 0.01$ indicated an extremely significant difference, $P \leq 0.05$ indicated a significant difference, and $P > 0.05$ indicated no significant difference. To adjust *P*-values without changing the significance threshold, the Benjamini-Hochberg (BH) method was applied, referred to as "Padjust" (Mu et al., 2020). Padjust is only applied in transcriptome data that require higher levels of significance (Liu et al., 2024).

3 Results

3.1 Growth performance

The body indices and growth performance of turbot after 40 days of hyperoxic and hypoxic treatment are presented in Figure 1. Overall, hyperoxia improved growth metrics, while hypoxia impaired them. Regarding body indices, the final body length (FBL) and final body weight (FBW) were significantly lowest in the LF group ($P < 0.05$) and significantly highest in the HF group ($P < 0.05$). Significant differences were also observed in the visceral somatic index (VSI), intestinal somatic index (ISI), and liver somatic index (LVI) between the LF and NF groups ($P < 0.05$), while no significant differences were noted in these visceral indices between the HF and NF groups ($P > 0.05$). These indices suggest that hypoxia negatively impacts organ development,

which may reflect physiological stress under hypoxic conditions (Figure 1A). In terms of growth performance, as the dissolved oxygen (DO) level increased, body weight gain (BWG), survival rate (SR), specific growth rate (SGR), and coefficient of fatness (CF) also increased, while feed conversion rate (FCR) and respiratory rate (RR) decreased. The HF group showed the highest values for these parameters, with significant differences ($P < 0.05$) (Figure 1B).

3.2 Intestinal microbiome: community abundance

At the phylum level, the five dominant phyla were Proteobacteria, Actinobacteriota, Bacteroidota, Firmicutes, and Patescibacteria. These dominant phyla play crucial roles in nutrient absorption, immunity, and metabolic processes, all of which are essential for adapting to DO fluctuations. Proteobacteria was the dominant phylum across all groups, with its abundance decreasing in the LF group. Firmicutes accounted for a high proportion only in the NF group, while Actinobacteriota showed increased abundance specifically in the HF group. Bacteroidota remained consistent across all groups (Figure 2A). The Circos plot illustrates phylum level, with outer ribbon colors indicating groups and inner ribbon colors indicating phyla. It provides a detailed breakdown of the abundance ratios of these phyla in each group. Acidobacteriota was present in both the LF and HF groups but absent in the NF group, possibly contributing to the reduced abundance of Firmicutes in the LF and HF groups due to competitive interactions. Additionally, several particular phyla, such as Cyanobacteria and Fusobacteriota, were uniquely detected in the LF group (Figure 2B).

At the genus level, the five dominant genera included Acinetobacter, Perlucidibaca, Sphingomonas, Bradyrhizobium, and Pelomonas. Overall, hyperoxia did not negatively impact the intestinal microbiome of turbot, while hypoxia led to an increase in intestinal bacteria, including a notable rise in potentially pathogenic bacteria such as Vibrio. The abundance of Acinetobacter and Perlucidibaca was lowest in the NF group, while Sphingomonas showed significantly lower abundance in the LF group. In contrast, the abundance of Vibrio significantly increased in the LF group (Figure 2C). The ternary phase diagram illustrates the differences between the three groups at the family level, along with bacterial abundance at the genus level within these families. Most genera are located near the center of the diagram, indicating that overall differences in bacterial abundance at the genus level between the groups were not significant. Additionally, the family Rhodocyclaceae showed increased abundance in the HF group (Figure 2D).

3.3 Intestinal microbiome: OTU clustering, functional prediction, and alpha diversity

In the OTU clustering analysis, 32 OTUs were shared by all three groups. The NF and HF groups each had more than 20 unique OTUs. However, the LF group showed an abnormal increase, with 84 unique OTUs (Figure 3A). In the microbiome-based KEGG pathway analysis, the LF group exhibited decreased microbial metabolism in diverse environments, while the HF group showed an increase. Other metabolic pathways were not significantly different between the NF and HF groups but were enriched in the LF group. These included pathways such as biosynthesis of amino acids, carbon metabolism, two-component systems, ATP-binding cassette (ABC) transporters, quorum sensing, ribosome activity, and purine metabolism. No significant differences in metabolic pathways were observed between the NF and HF groups (Figure 3B). The alpha diversity index showed no significant differences between the NF and HF groups. However, the LF group displayed a significantly higher diversity index, with metrics such as Sobs, Ace, Chao, and Jack indices being more than double those of the other two groups. Overall, hyperoxia had minimal impact on bacterial diversity and OTU composition, while hypoxia resulted in a significant increase in OTU composition and an abnormal rise in diversity (Table 2).

3.4 Transcriptome: sequencing and mapping of reads

Transcriptome analysis was conducted using the NF group as the control and the HF group as the experimental group. A total of

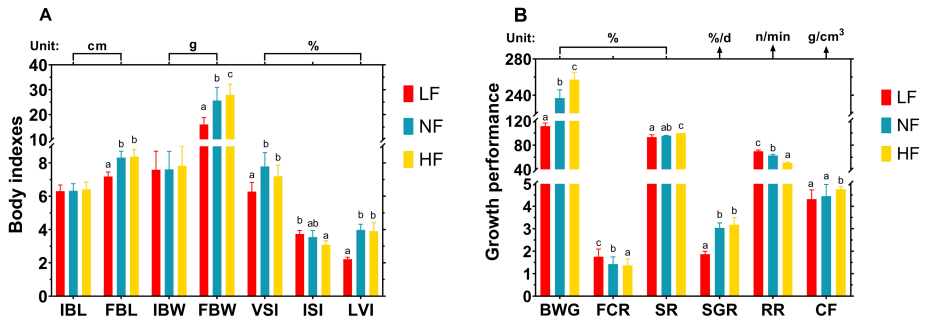

FIGURE 1
Effects of continuous hypoxia and hyperoxia exposure on turbot body indicators and growth performance over 40 days. **(A)** Body indicators. **(B)** Growth performance. IBL, initial body length; FBL, final body length; IBW, initial body weight; FBW, final body weight; VSI, visceral index; ISI, intestinal index; LVI, liver index; BWG, body weight gain; FCR, feed conversion rate; SR, survival rate; SGR, specific growth rate; RR, respiratory rate; CF, coefficient of fatness. Different superscript letters mean a significant difference ($P < 0.05$).

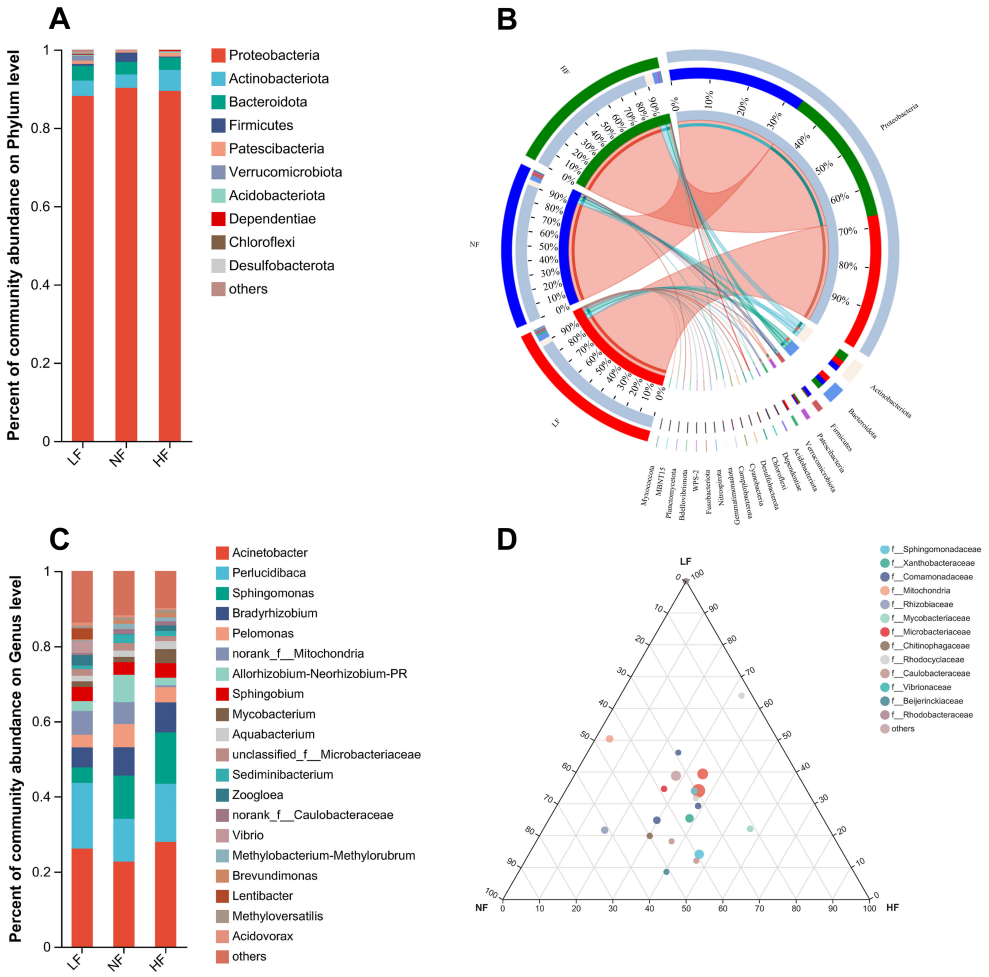

FIGURE 2
Community abundance of the intestinal microbiome at the phylum and genus levels. **(A)** Stacked histogram representing phylum level abundance. **(B)** Circos plot illustrating phylum level, with outer ribbon colors indicating groups and inner ribbon colors indicating phyla. **(C)** Stacked histogram depicting genus level abundance. **(D)** Ternary diagram at the genus level, where each corner represents a group, and each circle denotes a genus; larger circles indicate higher abundance of the corresponding genus.

six samples were analyzed, yielding 40.67 GB of clean data. Post-mapping quality control was verified to ensure consistent sequencing depth and alignment quality. Each sample produced over 6.1 GB of clean data, with more than 95.11% of bases having a Q30 quality score. Q30 refers to the percentage of bases with a sequencing quality score greater than 99.9% in relation to the total number of bases. The clean reads from each sample were mapped to the reference genome, with alignment rates ranging from 94.95% to 95.64%. In total, 22,861 expressed genes were detected, including 22,601 known genes and 260 newly identified genes. Additionally, 58,837 transcripts were expressed, comprising 46,318 known transcripts and 12,519 new transcripts. GO annotation covered 74% of the genes, while KEGG annotation covered 76%.

There was no significant difference in the overall gene expression distribution between the HF and NF groups (Figure 4A). However, 304 differentially expressed genes (DEGs) were identified, with 143 genes up-regulated and 161 genes down-regulated in the HF group. The identified DEGs likely play roles in oxygen transport, cellular repair, and metabolic adaptation under hyperoxic conditions (Figure 4B). The clustering heat map of DEGs showed that the three samples within each group were highly correlated, and there was a clear distinction in gene expression between the NF and HF groups (Figure 4C). Principal component analysis (PCA) further validated the distinction between the two groups, with similar distributions among the three samples within each group and significant separation between the NF and HF groups, indicating strong sample reproducibility and the substantial effect of experimental variables (Figure 4D).

3.5 Transcriptome: DEGs annotation and enrichment

The DEGs annotation and enrichment of turbot at hyperoxia are depicted in Figure 5. The GO annotation primarily focuses on three levels: cellular component, molecular function, and biological process. It mainly annotates processes related to the immune system, localization, response to stimuli, antioxidant activity,

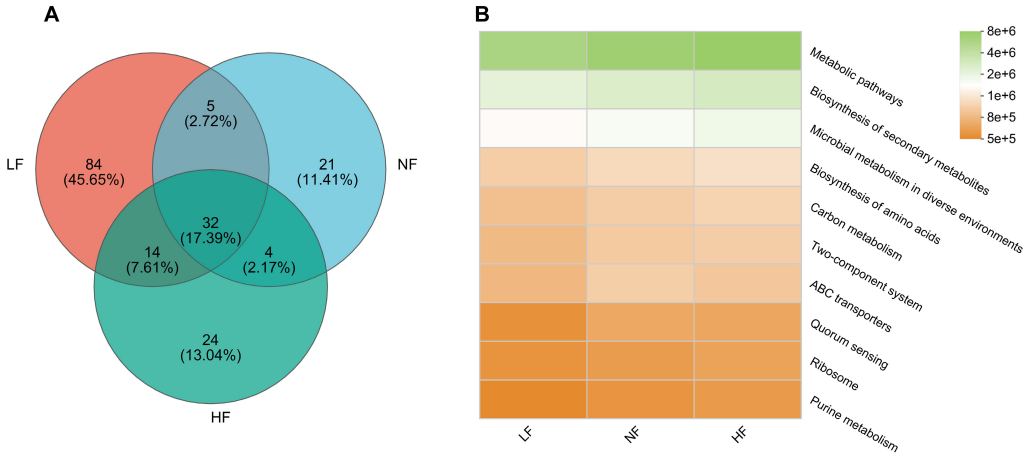

FIGURE 3
OTUs correlations and functional predictions. **(A)** Venn diagram showing shared OTUs. **(B)** Heatmap of KEGG pathway functional predictions (level 3). Color intensity within the same pathway across groups reflects variations in pathway enrichment.

transcription regulator activity, ATP-dependent activity, and molecular function regulation (Figure 5A). GO enrichment displays the top 20 GO terms with the most significant differences, including steroid metabolic processes (GO:0008202), extracellular space (GO:0005615), serine hydrolase activity (GO:0017171), endopeptidase activity (GO:0004175), creatine biosynthetic and metabolic processes (GO:0006601; GO:0006600), cholesterol biosynthetic process (GO:0006695), proteolysis, heme binding (GO:0020037), etc. (Figure 5B). GO enrichment demonstrates the importance of enzyme activity, biosynthesis, and metabolic processes in adapting to hyperoxia.

In hyperoxia, KEGG pathway annotation includes various aspects: immune system, endocrine system, transport and catabolism, cell growth and death, signaling molecules and interactions, signal transduction, carbohydrate metabolism, lipid metabolism, amino acid metabolism, etc. (Figure 5C). The KEGG pathway enrichment showed the most significant 25 pathways, including pancreatic secretion (map04972), steroid biosynthesis (map00100), protein digestion and absorption (map04974), glycine, serine, and threonine metabolism (map00260), arginine and proline metabolism (map00330), antigen processing and presentation (map04612), PPAR signaling pathway (map03320), fat digestion and absorption (map04975), hematopoietic cell lineage (map04640), calcium signaling pathway (map04020), etc. (Figure 5D). In the regulation mechanism of pancreatic secretion, it can be seen that carbon balance (CO_2, HCO_3^-) and ion balance (Cl^-, Na^+, K^+, Ca^{2+}) indirectly affected the genes regulating pancreatic secretion, resulting in significant up-regulation of the ATP gene family and the PMCA gene family (Figure 6). In addition, there are also differences in hematopoietic cell lineage, which prompted this study to conduct hematological experiments to verify the reliability of the enrichment pathway.

In hypoxia, previous studies have identified KEGG pathways that have been reported to be enriched of turbot, including antioxidant, HIF-1α pathway, glycolysis, gluconeogenesis, lipolysis, protein synthesis, water reabsorption, amino acid metabolism, nitrogen metabolism, ferroptosis, cell apoptosis, ion transport, calcium signaling pathway, PPAR signaling pathway, MAPK signaling pathway, primary immunodeficiency, etc (Guo et al., 2024; Ma et al., 2024). Comparing the hyperoxia adaptation pathway found in this study with the hypoxia adaptation pathway found by predecessors, it can be found that the pathways that play a role in hyperoxia and hypoxia adaptation are as follows: amino acid metabolism, antioxidation, protein metabolism, lipid metabolism, carbohydrate metabolism, PPAR signaling pathway, calcium signaling pathway, cell death, etc.

3.6 RT-qPCR verification of the DO adaptation genes

To enhance the reliability of the transcriptome data under hyperoxic conditions, this study employed dual validation. On one hand, the top 10 most significantly differentially expressed genes (DEGs) were validated; on the other hand, eight target genes associated with DO adaptation were selected for validation, with a focus on their expression across the LF, NF, and HF groups. The top 10 DEGs included *LOC5547*, *TG1*, *IIP44*, *EPOD*, *GTP7*, *MYH1s*,

TABLE 2 Intestinal microbiota diversity index statistics.

Groups	sobs	shannon	simpson	ace	chao	jack	pd	Pielou_e
LF	135.00	3.10	0.11	136.46	136.25	140.00	17.96	0.63
NF	62.00	2.92	0.09	62.00	62.00	62.00	10.07	0.71
HF	74.00	2.80	0.12	74.59	74.33	60.00	12.44	0.65

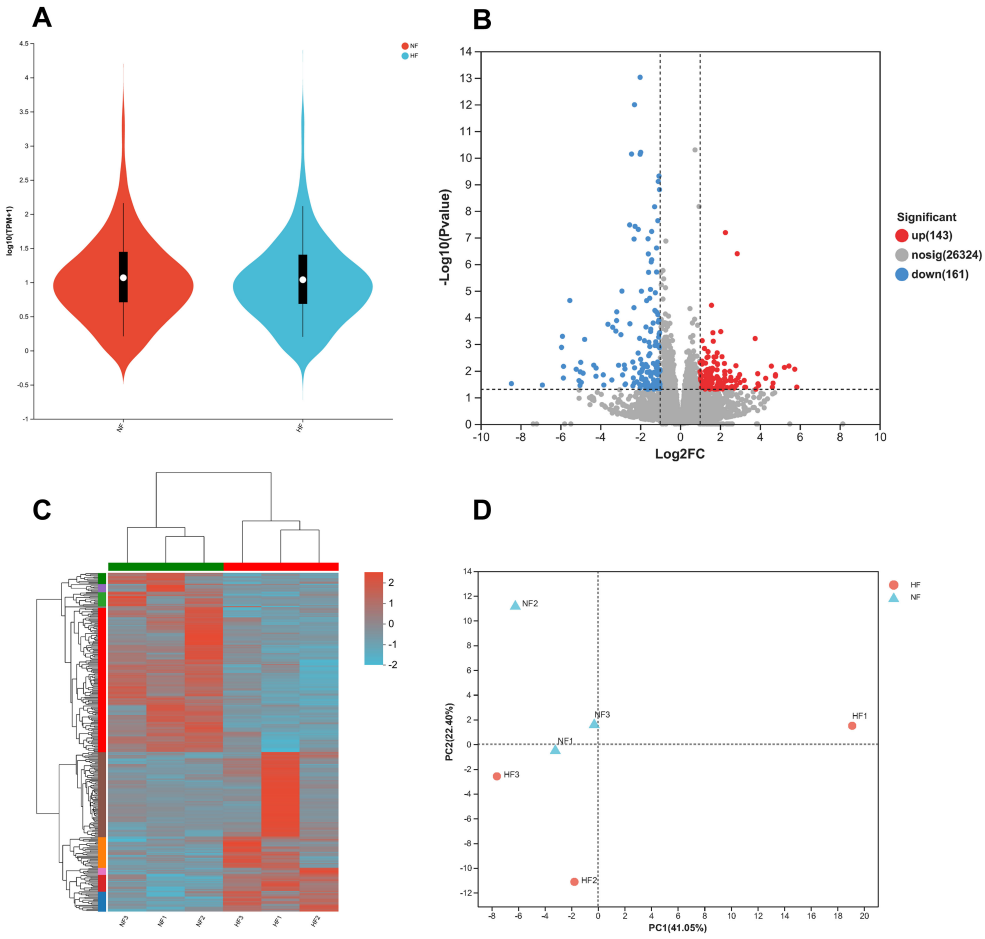

FIGURE 4
Distribution and relevance of RNA-seq data. **(A)** Distribution of expression levels for transcriptome sequencing genes. **(B)** Volcano plot showing differentially expressed genes (DEGs). **(C)** Clustering heatmap of DEGs, with the horizontal axis representing sample names and the vertical axis showing normalized FPKM values. Red indicates higher expression levels, while green indicates lower expression. **(D)** Principal Component Analysis (PCA) of samples, where closer proximity of points indicates greater similarity between samples.

PA2LY6, *Mucin5*, *FNDC7*, and *NOS1*. The RT-qPCR results were highly consistent with the RNA-seq data, both in terms of statistical significance and expression trends, confirming the reliability of the transcriptome data under hyperoxic conditions (Figure 7A). The eight target genes that play key roles in various biological pathways include energy metabolism (*ATP6*, *ATP8*), oxygen transport and regulation (*COX1*, *HIF1*, *Hbae5*, *CYP450*), antiviral and anticancer activity (*Man-SL*), and stress response (*HSP90*). Notably, the oxygen transport and regulation genes are also linked to energy metabolism. In the comparison of HF vs. NF, RT-qPCR was performed on the selected 8 target genes associated with DO, and the results were highly consistent with the RNA-seq data, further confirming the reliability of the transcriptome sequencing under high-oxygen conditions (Figure 7B). In the specific RT-qPCR results, no significant differences were observed in the relative expression of *ATP8*, *COX1*, and *HIF1* between the HF and NF groups ($P > 0.05$). In the LF group, the expression levels of *ATP6*, *HIF1*, *HSP90*, and *CYP450* were significantly higher ($P < 0.05$), while *COX1*, *Hbae5*, and *Man-SL* showed the lowest expression levels. In contrast, *Man-SL* expression reached a very high level in the HF group. Overall, as the DO level increased, the expression levels of *COX1*, *Hbae5*, and *Man-SL* gradually increased, while the expression levels of *HIF1*, *HSP90*, and *CYP450* progressively decreased (Figure 7C).

3.7 Hematological responses

To investigate how turbot blood adapts to varying DO levels, we conducted hematological analyses, focusing on four main aspects: routine tests, gas and ion balance, metabolic indicators, and enzyme activity. These metrics collectively provide insights into the physiological adjustments in blood composition and metabolic function required to maintain homeostasis under varying DO levels (Figure 8). In the blood routine test, the LF group showed a significant increase in white blood cells (WBC) ($P < 0.05$), with WBC reaching 31.51×10^9 cells/L, while platelet (PLT) counts significantly decreased ($P < 0.05$). As DO levels increased, total protein (TP), albumin (ALB), globulin (GLOB), and hematocrit (HCT) values also rose progressively ($P < 0.05$). Additionally, red blood cell (RBC) and hemoglobin (HGB) levels were significantly higher in both the LF and HF groups compared to the NF group (*P*

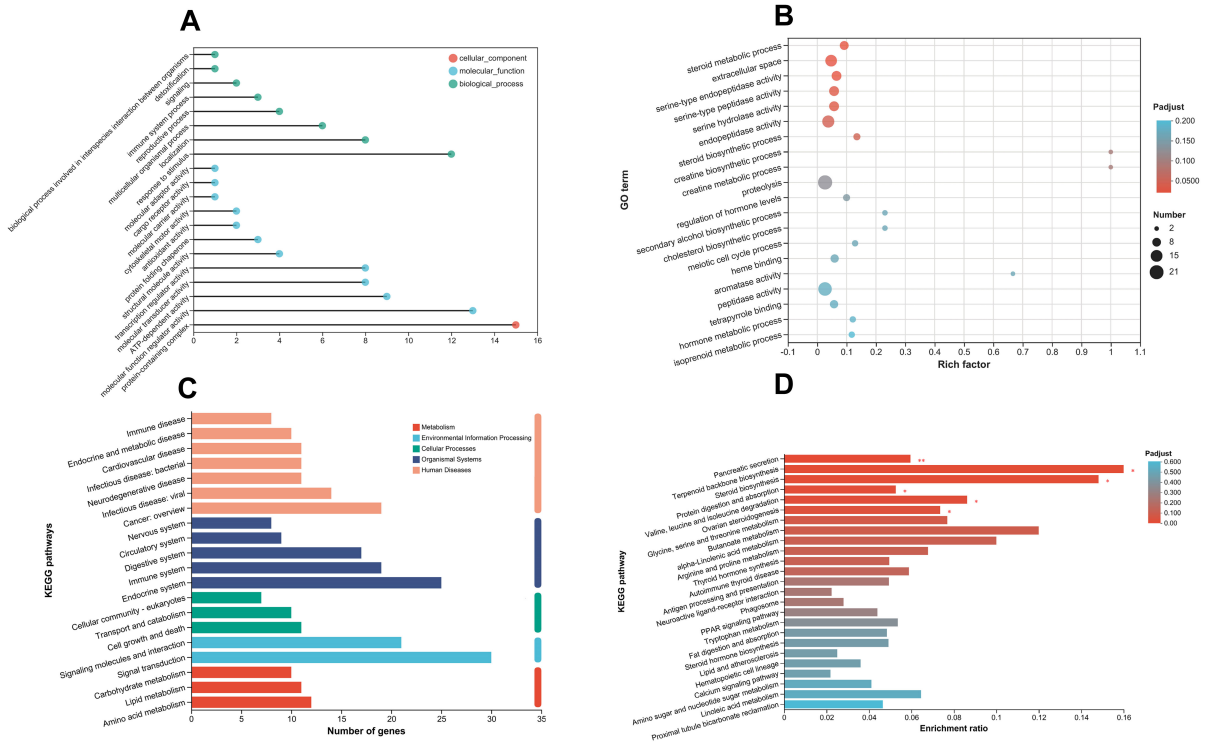

FIGURE 5
Annotation and enrichment of differentially expressed genes (DEGs). **(A)** Gene Ontology (GO) annotations, with the horizontal axis representing the number of annotated DEGs. **(B)** GO enrichment analysis, where the rich factor reflects the proportion of enriched genes relative to the total number of DEGs. **(C)** KEGG pathway annotations, with the horizontal axis indicating the number of genes or transcripts assigned to each pathway. **(D)** KEGG pathway enrichment analysis, highlighting the 25 most significant pathways. The horizontal axis shows the ratio of annotated DEGs in each KEGG pathway relative to the total DEGs.

< 0.05), particularly in the HF group ($P < 0.05$). Increased RBC and HGB levels suggest enhanced oxygen transport capacity, likely responding to the signal for oxygen delivery under both hypoxic and hyperoxic conditions (Figure 8A).

In the blood gas and ion balance, "P" represents partial pressure, while "C" denotes concentration. The LF group displayed significantly lower levels of $P(O_2)$, $P(CO_2)$, $C(CO_2)$, and C (HCO_3) ($P < 0.05$), indicating a well-maintained carbon balance at remarkably low levels. Across all groups, as DO levels increased, oxygen saturation ($S(O_2)$) remained constant, but $P(O_2)$ and total oxygen content ($C(tO_2e)$) significantly rose ($P < 0.05$), reflecting higher DO levels and a corresponding increase in total oxygen concentration in turbot blood. Additionally, adaptive changes in ion concentrations (Cl^-, H^+, K^+, Na^+, Ca^{2+}) were observed in response to DO variations (Figure 8B). Pancreatic secretion exhibited the most pronounced differences in adaptation to hyperoxia, with ion and carbon balance playing key roles in its regulatory mechanisms. The blood gas balance further supports the presence of these adaptive changes.

In the blood metabolic indicators, as DO levels increased, glucose (GLU) levels rose, while creatinine (CRE) decreased ($P < 0.05$). Compared to the NF group, the HF group showed significantly lower cholesterol (CHO) and CRE levels ($P < 0.05$), but significantly higher levels of GLU, blood urea nitrogen (BUN), and malondialdehyde (MDA) ($P < 0.05$). In the LF group, compared to the NF group, triglycerides (TG), BUN, CRE, and MDA levels were significantly elevated, while GLU was significantly reduced ($P < 0.05$). These changes in blood biochemical parameters suggest that metabolic regulation under hypoxia and hyperoxia differs, though both BUN and MDA consistently showed significant increases ($P < 0.05$) (Figure 8C).

In the blood enzyme activity, four enzymes related to non-specific immunity were assessed: acid phosphatase (ACP), alkaline phosphatase (AKP), polyphenol oxidase (PPO), and lysozyme (LZM). Four enzymes involved in metabolism were also assessed: succinate dehydrogenase (SDH), lactate dehydrogenase (LDH), glutamic pyruvic transaminase (GPT), and glutamic oxaloacetic transaminase (GOT). Under both hypoxia and hyperoxia, SDH, PPO, and LZM activities were significantly elevated ($P < 0.05$), while ACP activity significantly decreased ($P < 0.05$). In the LF group, AKP activity was the lowest, while GOT and LDH activities were the highest ($P < 0.05$). In contrast, the HF group showed the lowest LDH activity and the highest PPO and LZM activities ($P < 0.05$) (Figure 8D).

4 Discussion

Dissolved oxygen (DO) levels are crucial for fish health (Wu S. et al., 2023). Low DO levels can lead to hypoxia, resulting in reduced food intake, stunted growth, or even death (Wang et al., 2023). The

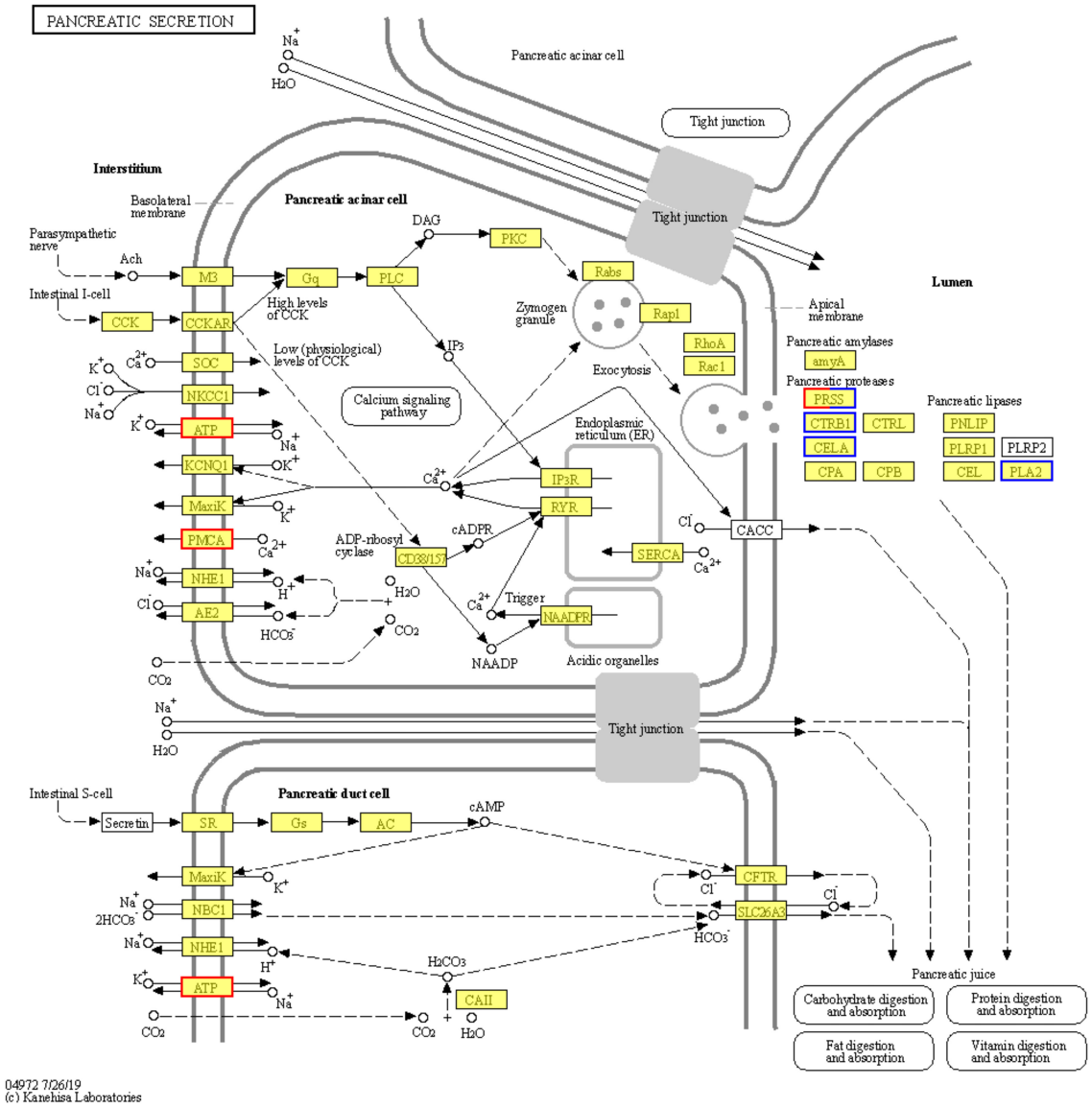

FIGURE 6
Regulation mechanisms of pancreatic secretion. The pancreatic secretion pathway (KEGG ID: map04972) shows the most significant differences in HF vs. NF. Border colors indicate gene expression changes, with red indicating upregulation, blue indicating downregulation, and a combination of both colors representing partial up- and down-regulation.

use of oxygen nanobubble (NB-O_2) technology in recirculating aquaculture systems (RAS) raises DO levels to hyperoxia, significantly enhancing the specific growth rate (SGR) and feed conversion rate (FCR) in grouper fish (Hanif et al., 2021). This study corroborates previous findings that hyperoxia produced by NB-O_2 technology significantly enhances turbot growth metrics, including SGR and FCR, demonstrating the positive impact of elevated DO on growth. In contrast, under hypoxic conditions (DO 3.5–5.0 mg/L), turbot shows low growth performance, characterized by low SGR and high FCR, compared to normoxic conditions (DO 7 mg/L) (Pichavant et al., 2000). This study is in line with previous studies about the impact of hypoxia on turbot. Under hypoxic conditions, turbots increase their respiratory rate (RR) to maintain oxygen intake (Maxime et al., 2000), whereas RR decreases in hyperoxia (Wu et al., 2016). This study supports the idea that lower RR under hyperoxic conditions is associated with more efficient oxygen uptake. Reportedly, DO tests were conducted on rainbow trout and turbot for longer than four weeks, growth performance was best at normoxia (DO 7.5 mg/L), when SGR and FCR were at the maximum and lowest, respectively; growth performance was lowest during long-term hypoxia (DO 3–5 mg/L). Reduced body weight gain (BWG), SGR, and increased FCR were among the negative effects of hyperoxia (DO 12–14 mg/L) on growth (Wu et al., 2016; Aksakal and Ekinci, 2021). Contrary to earlier research on hyperoxia in rainbow trout and turbot, this research indicates that hyperoxia fosters growth. Unlike traditional hyperoxic methods, such as air aeration or direct pure oxygen injection, which can sometimes harm fish, NB-O_2 technology

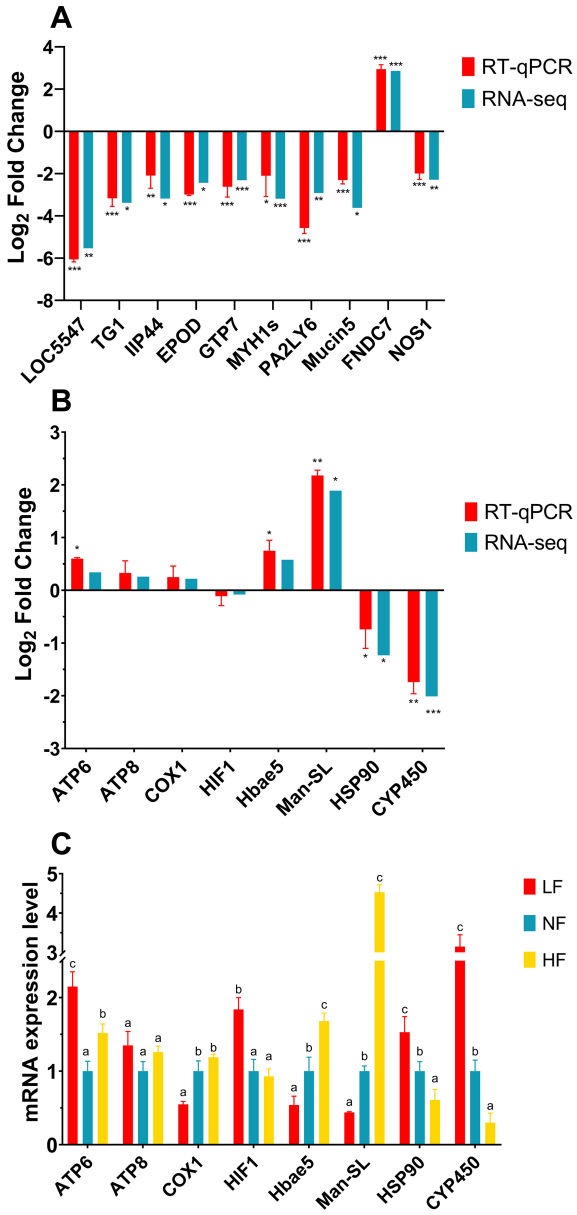

FIGURE 7
RT-qPCR verification and expression of dissolved oxygen (DO) adaptation genes. **(A)** Expression trends of the top 10 significantly differentially expressed genes (DEGs) from the HF vs. NF transcriptome in RT-qPCR and RNA-seq. **(B)** Expression trends of 8 DO-related target genes from the HF vs. NF transcriptome in RT-qPCR and RNA-seq. Significance is based on internal analysis of individual experiments, with significant differences marked by asterisks (*$P < 0.05$, **$P < 0.01$, ***$P < 0.001$). **(C)** Relative expression levels of 8 DO-related target genes in turbot gills, normalized to β-actin as an internal control. The NF group served as the control, with gene expression levels standardized to 1. Different superscript letters indicate significant differences ($P < 0.05$).

enhances oxygen availability through improved particle size and residence time (Ebina et al., 2013), also provides a stable, durable, and controlled DO level that supports safe and effective growth enhancement.

The intestinal microbiome is extremely important for fish health (Linh et al., 2023; Sanahuja et al., 2023), as it influences various physiological functions such as growth performance, vitamin synthesis, nutrient absorption, metabolic processes, immune responses, and acts as a barrier against infections (Dawood, 2021; Tan et al., 2022; Chen et al., 2024). The composition of the intestinal microbiome in marine fish is shaped by several factors, including developmental stage, diet, gender, trophic level, and habitat (Egerton et al., 2018). Previous studies have shown that the turbot's intestinal microbiome is primarily composed of Proteobacteria, Firmicutes, Cyanobacteria, Actinobacteriota, Bacteroidota, Acidobacteriota, and Gemmatimonadota (Li et al., 2022). In this study, it was observed that both hypoxia and hyperoxia did not disrupt the dominant bacterial phyla in turbot. However, under hypoxia, bacterial diversity in the intestine increased abnormally. These results are consistent with the findings of Linh et al (Linh et al., 2023). This is likely due to the fact that an anoxic environment often directly or indirectly alters intestinal microbiome composition and abundance, favoring the

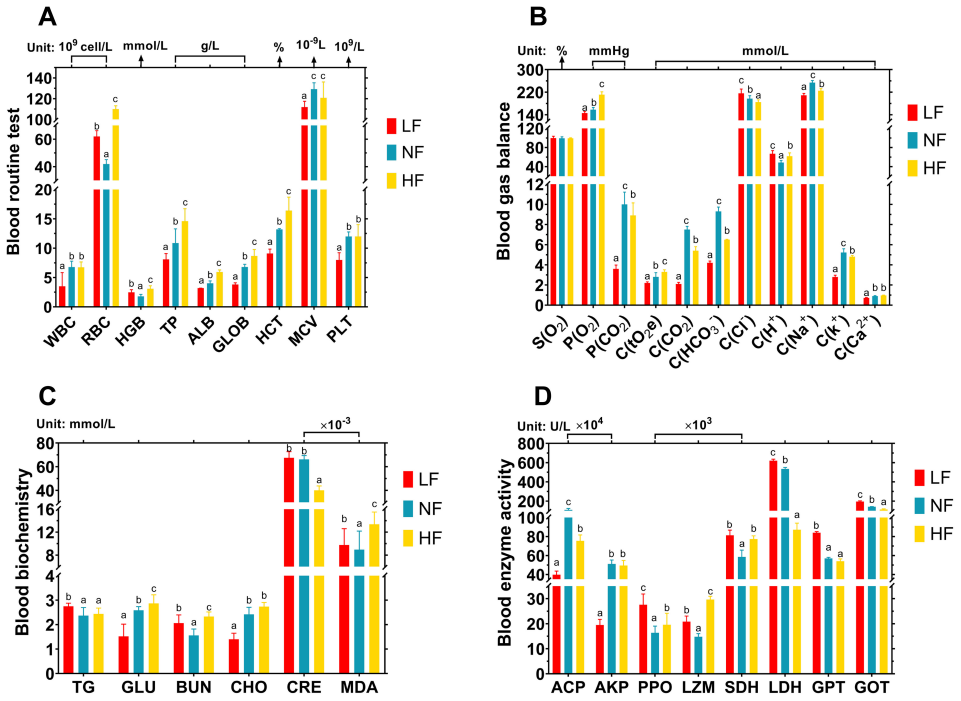

FIGURE 8
Effects of continuous hypoxia and hyperoxia exposure on turbot hematology over 40 days. **(A)** Blood routine test. WBC, white blood cells; RBC, red blood cells; HGB, hemoglobin; TP, total protein; ALB, albumin; GLOB, globulin; HCT, hematocrit; MCV, mean corpuscular volume; PLT, platelets. **(B)** Blood gas and ion balance. C(tO_2e), total oxygen concentration; S(O_2), oxygen saturation. Among the remaining indicators, P represents gas partial pressure, and C represents concentration. **(C)** Blood metabolic indicator. CHO, cholesterol; TG, triglycerides; GLU, glucose; BUN, blood urea nitrogen; CRE, creatinine; MDA, malondialdehyde. **(D)** Blood enzyme activity. ACP, acid phosphatase; AKP, alkaline phosphatase; PPO, polyphenol oxidase; LZM: lysozyme; LDH, lactate dehydrogenase; SDH, succinate dehydrogenase; GPT, glutamic pyruvic transaminase; GOT, glutamic oxalacetic transaminase. Different superscript letters mean a significant difference ($P < 0.05$).

survival and colonization of anaerobic bacteria (Han et al., 2021). In contrast, intestinal microbiome richness decreased under hyperoxia compared to hypoxia. Notably, Actinobacteriota, which are predominantly aerobic and capable of surviving in extreme environments, include several species that can produce antibiotics (Barka et al., 2015). This study found that the abundance of Actinobacteriota in the intestine of turbot increased under hyperoxia conditions, which is likely related to their survival characteristics. Acidobacteriota, commonly found in marine sediments, exhibit flexible respiratory pathways, including oxygen, nitrous oxide, metal oxides, and sulfur disproportionation, and can produce corresponding enzymes to reduce oxygen, nitrate, sulfide, and metal oxides (Flieder et al., 2021). In this study, Acidobacteriota was detected in the intestines of turbot only under hypoxia and hyperoxia, but not under normoxia, which may be linked to their oxygen regulation functions. Rhodocyclaceae, a member of the Proteobacteria family, involved in photosynthesis and nitrification with probiotic-like properties, has nutritional value and immune function (Oren, 2014). Previous research has shown that the use of NB-O_2 technology increased the abundance of Rhodocyclaceae in the intestines of Pacific white shrimp (*Litopenaeus vannamei*) (Xu et al., 2022), and this study similarly found an increase in Rhodocyclaceae in the intestine of turbot treated with NB-O_2. The increase in Rhodocyclaceae under hyperoxia may contribute to improved nutrient absorption and immune function, reflecting a beneficial adaptation to hyperoxia. The intestinal microbiome can regulate gas balance in the intestine through the peroxisome proliferator-activated receptor (PPAR) signaling pathway and various metabolic pathways (Vacca, 2017). Not only the PPAR signaling pathway but also KEGG pathway enrichment in this study confirmed the microbiome's important role in maintaining intestinal homeostasis.

Transcriptome analysis found a pathway for turbot to adapt to DO fluctuations. GO enrichment found that heme binding plays a crucial role in adapting hyperoxia. Heme binding regulates hemoglobin (HGB) synthesis, which in turn participates in the process of oxygen transport (Xie et al., 2024). The role of heme binding in hemoglobin synthesis emphasizes the need for efficient oxygen transport mechanisms under hyperoxia, underscoring the transcriptome's adaptive response to elevated DO. Pancreatic secretion, as the most significantly different KEGG enrichment pathway, is one of the important means for turbot to adapt to hyperoxia. The regulation of the balance of ions (e. g., Na^+, K^+, CI^-, HCO_3^-) secreted by the pancreas and the expression of the ATP gene family were verified by hematology and RT-qPCR in this study. In addition, the KEGG pathway of the intestinal microbiome revealed that metabolic pathways, carbon metabolism, amino acid synthesis, purine metabolism, and ATP-binding cassette (ABC) transporters are important pathways for adapting to DO fluctuations. Similarly, the KEGG results of the transcriptome showed that the pathways adapted to hyperoxia and hypoxia included amino acid metabolism,

antioxidant, protein metabolism, lipid metabolism, glucose metabolism, PPAR signaling pathway, calcium signaling pathway, apoptosis, etc. These pathways collectively facilitate the metabolic adjustment and cellular homeostasis necessary for turbot to cope with DO fluctuations, balancing energy demands and stress responses. It can be seen that the composition and function of the intestinal microbiome interact with gene regulation when the turbot undergoes DO fluctuation. In fact, not only turbot, most teleosts have similar pathways to adapt to changes in DO. For example, when the DO level is 2–4 mg/L, the up-regulation pathways of rainbow trout include amino acid metabolism, purine metabolism, ABC transporters, signal transduction, protein synthesis, PPAR signaling pathway, calcium signaling pathway, apoptosis, etc (Wu S. et al., 2023). Largemouth bass, *Micropterus salmoides*, also teleost fish, performed similarly under hypoxic conditions (Song et al., 2023). These data demonstrate the reliability of the pathways predicted in this study to adapt to DO fluctuations, and increase understanding how teleost fish adapt to DO fluctuations.

Hypoxia-inducible factor (*HIF*) plays a crucial role in adapting to DO fluctuations (Li J. et al., 2023). Specifically, *HIF1* regulates lactate dehydrogenase (LDH) activity, antioxidant defense, and apoptosis (Wu S. et al., 2023). Heat shock proteins (*HSPs*), a class of anti-stress genes, are activated in response to environmental stress (Garbuz, 2017). For example, *HSP70* is involved in ATP binding, ATPase activity, and unfolded protein binding (Liu et al., 2024). Cytochrome P450 (*CYP450*), an important heme-thiolate protein superfamily, plays a role in steroid metabolism, iron ion binding, and heme synthesis (Wang et al., 2020). Hemoglobin alpha embryonic 5 (*Hbae5*) regulates hemoglobin synthesis (Xie et al., 2024). Interestingly, this study found a negative correlation between the expression of *Hbae5* and *CYP450* as DO levels increased, suggesting a possible antagonistic relationship in the hemoglobin synthesis pathway. Previous research identified *HIF1*, *HSP70*, and *CYP450* as key genes for rainbow trout adaptation to hypoxia (Aksakal and Ekinci, 2021; Wu S. et al., 2023). Similarly, this study found that *HIF1*, *HSP90*, and *CYP450* are important for turbot's adaptation to hypoxia. However, *HIF1* does not play a significant role in hyperoxia. This is consistent with the observation that, like *HSP90*, *HSP70* expression remains unchanged in rainbow trout and Nile tilapia exposed to hyperoxia (Aksakal and Ekinci, 2021; Linh et al., 2023). These findings confirm that the stress response mechanisms differ between hyperoxia and hypoxia. Adenosine triphosphate (*ATP*) is essential for energy metabolism, with *ATP6* and *ATP8* playing key roles in ATP synthesis and mitochondrial assembly (Wang et al., 2018). This study showed that *ATP6* expression is upregulated in both hypoxia and hyperoxia, indicating that fish regulate energy metabolism to adapt to changing DO levels (Mu et al., 2020). Mannose-specific lectin (*Man-SL*), a non-immune carbohydrate-binding protein involved in antiviral and anticancer processes (Gupta et al., 2024), was highly expressed in hyperoxia and downregulated in hypoxia. This suggests that *Man-SL* may be linked to changes in glucose metabolism, potentially driving differences in carbohydrate metabolism under varying oxygen conditions.

Exposure to hypoxia can cause significant hematological changes in fish, affecting cell composition, electrolyte balance, and metabolic indicators (Gaulke et al., 2014). Red blood cells (RBC) play a vital role in transporting oxygen via hemoglobin (HGB), as well as in CO_2 transport and hydrogen ion buffering (Harvey, 2022). Hematocrit (HCT) represents the proportion of RBCs in the total blood volume (Bain, 2017). In previous studies, turbot exposed to three DO levels—hypoxia (2–5 mg/L), normoxia (7 mg/L), and hyperoxia (11–14 mg/L)—for six weeks showed elevated RBC, HGB, and HCT levels in both the hypoxia and hyperoxia groups compared to the control group at various time points (Wu et al., 2016). Similar results were observed in this study, the elevation of RBC and HGB in both hypoxic and hyperoxic groups reflects an adaptive mechanism to optimize oxygen delivery under diverse DO conditions, which is essential for maintaining metabolic stability. In this study, white blood cell (WBC) counts remained unaffected by hyperoxia but decreased under hypoxia. This confirmed findings in *Phoxinus lagowskii*, a cold-water fish, which also exhibited reduced WBC counts during hypoxia (Yang et al., 2021). This suggests that WBCs play a role in hypoxia adaptation and damage repair in fish. Albumin (ALB) and globulin (GLOB) are key proteins in fish blood. ALB maintains osmotic pressure and aids in the transport of various substances, while GLOB is involved in immune responses (Pastorino et al., 2022). In this study, hypoxia caused a decrease in ALB and GLOB levels in turbot, whereas these proteins increased under hyperoxia.

DO fluctuation can significantly affect the gas pressure and ion balance in the blood of marine fish (Montgomery et al., 2019). During hypoxia, for example, the concentration of carbon dioxide [$C(CO_2)$] in the blood decreases, as observed in grass carp (*Ctenopharyngodon idellus*) (Wu X. et al., 2023). Efficient CO_2 management under hypoxia prevents acidosis, helping to maintain blood pH homeostasis, a crucial aspect of metabolic balance in fish exposed to low DO. This study similarly found that both the partial pressure ($P(CO_2)$) and concentration ($C(CO_2)$) of carbon dioxide in turbot blood were markedly low during hypoxia. This reduction can be attributed to anaerobic respiration, which produces not only CO_2 but also metabolites such as lactic acid and ethanol (Wang et al., 2023). As DO levels rise, both the oxygen pressure ($P(O_2)$) and total oxygen concentration ($C(tO_2e)$) increase, although oxygen saturation ($S(O_2)$) remains constant. When DO reaches hyperoxic levels, $P(O_2)$ and $P(CO_2)$ exhibit an inverse, complementary relationship to maintain gas pressure equilibrium. Blood electron neutrality and acid-base balance are maintained through the exchange of equal amounts of HCO_3^-, Cl^-, H^+, and Na^+ with the surrounding environment (Nam and Park, 2020). This study identified distinct regulatory patterns of ions such as HCO_3^-, Cl^-, H^+, K^+, Ca^{2+}, and Na^+ across the three experimental groups, which contribute to maintaining pH homeostasis. These findings emphasize the remarkable ability of turbot to regulate blood acid-base balance under varying DO conditions (Pichavant et al., 2000; Li et al., 2019).

Immunity can be classified into two types: specific and non-specific, both of which are vital defense mechanisms for animals during infection, drug use, toxin exposure, and environmental changes (Dierick et al., 2024). Non-specific immune responses involve certain enzymes, including acid phosphatase (ACP), alkaline phosphatase (AKP), phenoloxidase (PPO), and lysozyme (LZM) (Guo et al., 2024). This study found that hypoxia led to a decrease in ACP and

AKP activity, which is unfavorable for immune defense; however, under hyperoxia, the overall activity of these immune enzymes increased, suggesting a more favorable immune response. Metabolic enzymes, such as lactate dehydrogenase (LDH), succinate dehydrogenase (SDH), glutamic pyruvic transaminase (GPT), and glutamic oxalacetic transaminase (GOT), play critical roles in energy metabolism in fish (Li et al., 2019; Wu S. et al., 2023). Under hypoxia, glycogen in turbot is broken down into glucose (GLU), and then this GLU is metabolized anaerobically into lactic acid, leading to lactic acid accumulation. LDH is involved in the glycolysis pathway, which increases LDH activity to process the excess lactic acid (Pichavant et al., 2002; Wu et al., 2016; Ma et al., 2024). This study confirmed this process. SDH is a key enzyme in the tricarboxylic acid (TCA) cycle, promoting ATP production (Li W. et al., 2023), while GPT and GOT are involved in amino acid metabolism and catalyze the production of α-ketoglutarate, a TCA cycle intermediate (Tamber et al., 2023). During hypoxia, turbot displays the GOT and GPT activity increases (Ma et al., 2024). Analogous, this study revealed that changes in DO levels affected the activities of SDH, GPT, and GOT, confirming that DO fluctuations influence both energy and amino acid metabolism in turbot. In this study, hyperoxia exerts a more positive effect on non-specific immune responses and metabolic processes in turbot compared to hypoxia.

Blood metabolic indices provide a perspective on the internal metabolism of oxygen concentration changes (Wu et al., 2016). Glucose (GLU) is an important energy-supplying monosaccharide and is influenced by blood oxygen levels; triglyceride (TG) represents fats in the blood; cholesterol (CHO) is involved in hormone synthesis, lipid digestion, and vitamin absorption; malondialdehyde (MDA) is a byproduct of lipid peroxidation; blood urea nitrogen (BUN) is a byproduct of protein metabolism; and creatinine (CRE) is produced from creatine metabolism (Jiang et al., 2018; Ma et al., 2023; Chen et al., 2025). This study found that the metabolic levels of certain substances, such as GLU, TG, CHO, and CRE, varied between hypoxia and hyperoxia, likely due to the differences between anaerobic and aerobic respiration pathways. These metabolic differences help explain the variations in growth performance. Under hyperoxia, this study found an accumulation of GLU in the blood; under hypoxia, GLU reduction, a similar GLU reduction phenomenon was observed in juvenile great sturgeon (*Huso huso*) (Falahatkar et al., 2013). GLU appears to be influenced by blood oxygen levels but is actually regulated by insulin (Ma et al., 2023). Insulin secretion, in turn, is affected by pancreatic secretion pathways, which confirms that pancreatic secretion is a key pathway for adaptating to hyperoxia. GLU regulation represents another important aspect of this pathway. Of concern, both hypoxia and hyperoxia led to increases in MDA and BUN (though not exponentially), indicating potential cellular damage. This suggests that the physiological adaptation to DO fluctuations may come at the cost of some damage. Previous studies have shown that hypoxia increases levels of total protein (TP), TG, CHO, and MDA in turbot blood, pointing to accelerated metabolism, abnormal lipid metabolism, and liver damage under hypoxia (Ma et al., 2024; Chen et al., 2025). This study confirms similar findings, reinforcing the idea that hypoxia negatively impacts metabolism and liver function.

5 Conclusion

This study investigated the effects of NB-O_2-induced hyperoxia and hypoxia on turbot growth, intestinal microbiome, and physiological adaptations, revealing the hypoxic drawbacks and hyperoxic benefits. Concretely, in RAS, the hyperoxia generated by NB-O_2 technology significantly enhanced turbot growth, preserved the composition of the intestinal microbiome, and increased the abundance of beneficial intestinal probiotics. In contrast, hypoxia hindered growth, led to an abnormal increase in intestinal microbiome diversity, and pointed to the disruption of nutrient metabolism and intestinal microbiota homeostasis. The KEGG pathways for adaptation to hyperoxia and hypoxia differ: amino acid metabolism and the PPAR signaling pathway are involved in both, but pancreatic secretion plays a key role in hyperoxia adaptation, while the HIF-1α pathway is crucial for hypoxia adaptation. The distinct pathways for hyperoxia and hypoxia adaptation reveal targeted physiological and metabolic adjustments, underscoring the complexity of turbot responses to variable DO levels in aquaculture. Hematological analysis also revealed distinct changes under hyperoxia and hypoxia, such as electrolyte balance, hemoglobin (HGB), glucose (GLU), and non-specific immune enzymes (ACP, AKP, PPO, LZM). These hematological changes highlight turbot's ability to maintain oxygen transport and immune function across different oxygen conditions, critical for survival in variable aquaculture environments. In brief, these findings suggest that NB-O_2 technology holds promise for optimizing growth and health in turbot aquaculture by using RAS. Future research should explore long-term impacts of hyperoxia on other physiological systems and assess optimal DO levels across different developmental stages.

Data availability statement

All available codes have been uploaded to Github, and the project numbers are PRJNA1159012 (https://github.com/YiChen-CNGZ/PRJNA1159012) and PRJNA1118073 (https://github.com/YiChen-CNGZ/PRJNA1118073).

Ethics statement

The animal study was approved by the Animal Experiment of Dalian Ocean University. The study was conducted in accordance with the local legislation and institutional requirements.

Author contributions

YC: Conceptualization, Data curation, Formal Analysis, Investigation, Methodology, Software, Validation, Writing – original draft, Writing – review & editing. YZ: Formal Analysis, Investigation, Methodology, Validation, Writing – review & editing. RZ: Formal Analysis, Investigation, Writing – review & editing. HD: Investigation, Methodology, Writing – review & editing. XM: Investigation, Methodology, Writing – review & editing. KI:

Resources, Writing – review & editing. TO: Resources, Writing – review & editing. XZ: Formal Analysis, Project administration, Writing – review & editing. YH: Funding acquisition, Project administration, Supervision, Visualization, Writing – review & editing. TR: Data curation, Project administration, Resources, Supervision, Writing – review & editing.

Funding

The author(s) declare that financial support was received for the research, authorship, and/or publication of this article. Supported by the Ministry of Science and Technology of the People's Republic of China, the National Key Research and Development Program of China (No. 2022YFE0117900); Project of the Educational Department of Liaoning Province (No. LJKMZ20221121).

Acknowledgments

We would like to express gratitude to all individuals mentioned in the article, as well as the laboratory staff and other personnel who provided assistance, especially Professors Zhao, Ren and Han.

Conflict of interest

Authors KI and TO were employed by Iwatani Co., Ltd. Japan.

The remaining authors declare that the research was conducted in the absence of any commercial or financial relationships that could be construed as a potential conflict of interest.

Generative AI statement

The authors declare that no Generative AI was used in the creation of this manuscript.

Publisher's note

References

Agarwal, A., Ng, W. J., and Liu, Y. (2011). Principle and applications of microbubble and nanobubble technology for water treatment. *Chemosphere* 84, 1175–1180. doi: 10.1016/j.chemosphere.2011.05.054

Ahmed, N., and Turchini, G. M. (2021). Recirculating aquaculture systems (RAS): Environmental solution and climate change adaptation. *J. Clean. Prod.* 297, 126604. doi: 10.1016/j.jclepro.2021.126604

Aksakal, E., and Ekinci, D. (2021). Effects of hypoxia and hyperoxia on growth parameters and transcription levels of growth, immune system and stress related genes in rainbow trout. *Comp. Biochem. Physiol. A: Mol. Integr. Physiol.* 262, 111060. doi: 10.1016/j.cbpa.2021.111060

Anders, S., and Huber, W. (2010). Differential expression analysis for sequence count data. *Genome Biol.* 11, R106. doi: 10.1186/gb-2010-11-10-r106

Badiola, M., Basurko, O. C., Piedrahita, R., Hundley, P., and Mendiola, D. (2018). Energy use in recirculating aquaculture systems (RAS): a review. *Aquacult. Eng.* 81, 57–70. doi: 10.1016/j.aquaeng.2018.03.003

Bain, B. J. (2017). Structure and function of red and white blood cells. *Medicine* 45, 187–193. doi: 10.1016/j.mpmed.2017.01.011

Bao, B. (2022). "General Introduction of Flatfish Metamorphosis," in *Flatfish Metamorphosis*. Ed. B. Bao (Springer Nature Singapore, Singapore), 1–37. doi: 10.1007/978-981-19-7859-3_1

Barka, E. A., Vatsa, P., Sanchez, L., Gaveau-Vaillant, N., Jacquard, C., Klenk, H.-P., et al. (2015). Taxonomy, physiology, and natural products of actinobacteria. *Microbiol. Mol. Biol. Rev.* 80, 1–43. doi: 10.1128/MMBR.00019-15

Chen, S. (2023). Ultrafast one-pass FASTQ data preprocessing, quality control, and deduplication using fastp. *iMeta* 2, e107. doi: 10.1002/imt2.107

Chen, Y., Cui, S., Wu, L., Han, Y., Zhao, X., and Ren, T. (2024). Dietary silicate minerals relieving cadmium or lead poisoning in juvenile sea cucumber, *Apostichopus japonicus*. *Mar. Environ. Res.* 202, 106795. doi: 10.1016/j.marenvres.2024.106795

Chen, S., Wang, F., Song, J., Li, F., Wang, J., and Jia, Y. (2025). Sexual dimorphism in physiological responses of turbot (*Scophthalmus maximus L.*) under acute hypoxia and reoxygenation. *Aquaculture* 595, 741614. doi: 10.1016/j.aquaculture.2024.741614

Dawood, M. A. O. (2021). Nutritional immunity of fish intestines: important insights for sustainable aquaculture. *Rev. Aquacult.* 13, 642–663. doi: 10.1111/raq.12492

Dierick, M., Ongena, R., Vanrompay, D., Devriendt, B., and Cox, E. (2024). Exploring the modulatory role of bovine lactoferrin on the microbiome and the immune response in healthy and Shiga toxin-producing *E. coli* challenged weaned piglets. *J. Anim. Sci. Biotechnol.* 15, 39. doi: 10.1186/s40104-023-00985-3

Ebina, K., Shi, K., Hirao, M., Hashimoto, J., Kawato, Y., Kaneshiro, S., et al. (2013). Oxygen and air nanobubble water solution promote the growth of plants, fishes, and mice. *PloS One* 8, e65339. doi: 10.1371/journal.pone.0065339

Egerton, S., Culloty, S., Whooley, J., Stanton, C., and Ross, R. P. (2018). The gut microbiota of marine fish. *Front. Microbiol.* 9. doi: 10.3389/fmicb.2018.00873

Engle, C. R. (2023). The economics of recirculating aquaculture systems. *J. World Aquacult. Soc* 54, 782–785. doi: 10.1111/jwas.13004

Falahatkar, B., Lakani, F. B., and Sattari, M. (2013). Effect of different oxygen levels on growth performance, stress response and oxygen consumption in two weight groups of great sturgeon *Huso huso*. *Iran. J. Fish. Sci.* 12, 533–549. doi: 10.22092/ijfs.2018.114297

Flieder, M., Buongiorno, J., Herbold, C. W., Hausmann, B., Rattei, T., Lloyd, K. G., et al. (2021). Novel taxa of Acidobacteriota implicated in seafloor sulfur cycling. *ISME J.* 15, 3159–3180. doi: 10.1038/s41396-021-00992-0

Foudas, A. W., Kosheleva, R. I., Favvas, E. P., Kostoglou, M., Mitropoulos, A. C., and Kyzas, G. Z. (2023). Fundamentals and applications of nanobubbles: a review. *Chem. Eng. Res. Des.* 189, 64–86. doi: 10.1016/j.cherd.2022.11.013

Garbuz, D. (2017). Regulation of heat shock gene expression in response to stress. *Mol. Biol.* 51, 352–367. doi: 10.1134/S0026893317020108

Gaulke, G. L., Dennis, C. E., Wahl, D. H., and Suski, C. D. (2014). Acclimation to a low oxygen environment alters the hematology of largemouth bass (*Micropterus salmoides*). *Fish Physiol. Biochem.* 40, 129–140. doi: 10.1007/s10695-013-9830-6

Guo, Z., Meng, X., Zhang, Y., Wu, D., Zhang, R., Zhao, X., et al. (2024). Replacing sea mud with attachment of suspension cage can improve growth and gut health for sea cucumber *Apostichopus japonicus*. *Front. Mar. Sci.* 11. doi: 10.3389/fmars.2024.1452166

Guo, Z., Peng, Z., Zhang, Y., Meng, X., Wu, D., Zhang, R., et al. (2024). Effects of dietary fermented attachments of suspension cage as a replacement for sea mud on growth and intestinal health of sea cucumber *Apostichopus japonicus*. *Aquacult. Rep.* 38, 102313. doi: 10.1016/j.aqrep.2024.102313

Gupta, A., Yadav, K., Yadav, A., Ahmad, R., Srivastava, A., Kumar, D., et al. (2024). Mannose-specific plant and microbial lectins as antiviral agents: A review. *Glycoconj. J.* 41, 1–33. doi: 10.1007/s10719-023-10142-7

Han, N., Pan, Z., Liu, G., Yang, R., and Yujing, B. (2021). Hypoxia: the "invisible pusher" of gut microbiota. *Front. Microbiol.* 12. doi: 10.3389/fmicb.2021.690600

Hanif, I. M., Effendi, I., Budiardi, T., and Diatin, I. (2021). The recirculated aquaculture system (RAS) development with nanobubble application to improve

growth performance of grouper fish fry culture. *J. Akuakult. Indones.* 20, 181–190. doi: 10.19027/jai.20.2.181-190

Harvey, J. W. (2022). "Erythrocyte Biochemistry," in *Schalm's Veterinary Hematology*. New Jersey, USA: John Wiley&Sons Inc. 166–171. doi: 10.1002/9781119500537.ch21

Hays, H., Gu, Z., Mai, K., and Zhang, W. (2023). Transcriptome-based nutrigenomics analysis reveals the roles of dietary taurine in the muscle growth of juvenile turbot (*Scophthalmus maximus*). *Comp. Biochem. Physiol. D: Genomics Proteomics* 47, 101120. doi: 10.1016/j.cbd.2023.101120

Jiang, B., Qu, Z., Gu, Y., Li, X., Wang, J., Zhang, J., et al. (2018). Renoprotective effect of JinQi-JiangTang tablet on high-fat diet and low-dose streptozotocin-induced type 2 diabetic rats. *RSC Adv.* 8, 41858–41871. doi: 10.1039/c8ra07858k

Lee, C., Cheong, S., Lee, H. J., Kwon, M., Kang, I., Oh, E. G., et al. (2010). Evaluation of the sensitivity and specificity of primer pairs and the efficiency of RNA extraction procedures to improve noroviral detection from oysters by nested reverse transcription-polymerase chain reaction. *J. Microbiol.* 48, 586–593. doi: 10.1007/s12275-010-0047-4

Li, Z., Bao, N., Ren, T., Han, Y., Jiang, Z., Bai, Z., et al. (2019). The effect of a multi-strain probiotic on growth performance, non-specific immune response, and intestinal health of juvenile turbot. *Scophthalmus maximus L. Fish Physiol. Biochem.* 45, 1393–1407. doi: 10.1007/s10695-019-00635-4

Li, J., Li, Y., Liang, X., Yang, Z., Peng, Y., Zhang, Y., et al. (2023). Blood redistribution preferentially protects vital organs under hypoxic stress in Pelteobagrus vachelli. *Aquat. Toxicol.* 258, 106498. doi: 10.1016/j.aquatox.2023.106498

Li, W., Quan, L., Peng, K., Wang, Y., Wang, X., Chen, Q., et al. (2023). Succinate dehydrogenase is essential for epigenetic and metabolic homeostasis in hearts. *Basic Res. Cardiol.* 118, 45. doi: 10.1007/s00395-023-01015-z

Li, C., Tian, Y., Wang, L., Zhang, B., and Ma, Q. (2022). Effects of replacing fishmeal by raw or *Lactobacillus acidophilus*-fermented soybean meal on growth, intestinal digestive and immune-related enzyme activities, morphology, and microbiota in turbot (*Scophthalmus maximus L.*). *Aquacult. Nutr.* 2022, 2643235. doi: 10.1155/2022/2643235

Linh, N. V., Khongcharoen, N., Nguyen, D.-H., Dien, L. T., Rungrueng, N., Jhunkeaw, C., et al. (2023). Effects of hyperoxia during oxygen nanobubble treatment on innate immunity, growth performance, gill histology, and gut microbiome in Nile tilapia, *Oreochromis niloticus*. *Fish Shellfish Immunol.* 143, 109191. doi: 10.1016/j.fsi.2023.109191

Liu, T., Nie, H., Ding, J., Huo, Z., and Yan, X. (2024). Physiological and transcriptomic analysis provides new insights into osmoregulation mechanism of *Ruditapes philippinarum* under low and high salinity stress. *Sci. Total Environ.* 935, 173215. doi: 10.1016/j.scitotenv.2024.173215

Livak, K. J., and Schmittgen, T. D. (2001). Analysis of relative gene expression data using real-time quantitative PCR and the $2^{-\Delta\Delta CT}$ method. *Methods* 25, 402–408. doi: 10.1006/meth.2001.1262

Ma, Q., Xu, H., Limbu, S. M., Wei, Y., and Liang, M. (2023). Comparative analysis of glucose and fructose tolerance in two marine fishes: effects on insulin secretion and acute hypoxia tolerance. *Front. Mar. Sci.* 10. doi: 10.3389/fmars.2023.1310415

Ma, Q., Xu, H., Wei, Y., and Liang, M. (2024). Effects of acute hypoxia on nutrient metabolism and physiological function in turbot, *Scophthalmus maximus*. *Fish Physiol. Biochem.* 50, 367–383. doi: 10.1007/s10695-022-01154-5

Maxime, V., Pichavant, K., Boeuf, G., and Nonnotte, G. (2000). Effects of hypoxia on respiratory physiology of turbot, *Scophthalmus maximus*. *Fish Physiol. Biochem.* 22, 51–59. doi: 10.1023/a:1007829214826

Miranda, J., Veneza, I., Ferreira, C., Santana, P., Lutz, I., Furtado, C., et al. (2024). First neurotranscriptome of adults Tambaquis (*Colossoma macropomum*) with characterization and differential expression between males and females. *Sci. Rep.* 14, 3130. doi: 10.1038/s41598-024-53734-5

Montgomery, D. W., Simpson, S. D., Engelhard, G. H., Birchenough, S. N. R., and Wilson, R. W. (2019). Rising CO_2 enhances hypoxia tolerance in a marine fish. *Sci. Rep.* 9, 15152. doi: 10.1038/s41598-019-51572-4

Mortazavi, A., Williams, B. A., McCue, K., Schaeffer, L., and Wold, B. (2008). Mapping and quantifying mammalian transcriptomes by RNA-Seq. *Nat. Methods* 5, 621–628. doi: 10.1038/nmeth.1226

Mu, Y., Li, W., Wu, B., Chen, J., and Chen, X. (2020). Transcriptome analysis reveals new insights into immune response to hypoxia challenge of large yellow croaker (*Larimichthys crocea*). *Fish Shellfish Immunol.* 98, 738–747. doi: 10.1016/j.fsi.2019.11.021

Nam, S. S., and Park, H. Y. (2020). Effects of endurance exercise under hypoxia on acid-base and ion balance in healthy males. *Phys. Act. Nutr.* 24, 7–12. doi: 10.20463/pan.2020.0015

Naylor, R. L., Hardy, R. W., Buschmann, A. H., Bush, S. R., Cao, L., Klinger, D. H., et al. (2021). A 20-year retrospective review of global aquaculture. *Nat* 591, 551–563. doi: 10.1038/s41586-021-03308-6

Nghia, N. H., Nguyen, N. T., Binh, P. T., May, L. T., Huy, T. T., Giang, P. T., et al. (2022). Effect of nanobubbles (oxygen, ozone) on the Pacific white shrimp (*Penaeus vannamei*), *Vibrio parahaemolyticus* and water quality under lab conditions. *Fish Aquat. Sci.* 25, 429–440. doi: 10.47853/FAS.2022.e39

Nguyen, H. H. T., Jeong, Y. H., Choi, Y. H., and Kwak, D. H. (2024). Oxidation capacity evaluation of oxygen nanobubbles for dye wastewater treatment. *J. Water Process Eng.* 61, 105344. doi: 10.1016/j.jwpe.2024.105344

Oren, A. (2014). "The Family Rhodocyclaceae," in *The Prokaryotes: Alphaproteobacteria and Betaproteobacteria*. Eds. E. Rosenberg, E. F. DeLong, S. Lory, E. Stackebrandt and F. Thompson (Springer Berlin Heidelberg, Berlin, Heidelberg), 975–998. doi: 10.1007/978-3-642-30197-1_292

Pastorino, P., Bergagna, S., Vercelli, C., Pagliasso, G., Dellepiane, L., Renzi, M., et al. (2022). Changes in serum blood parameters in farmed rainbow trout (*Oncorhynchus mykiss*) fed with diets supplemented with waste derived from supercritical fluid extraction of sweet basil (*Ocimum basilicum*). *Fishes* 7, 89. doi: 10.3390/fishes7020089

Pichavant, K., Maxime, V., Thébault, M., Ollivier, H., and Nonnotte, G. (2002). Effects of hypoxia and subsequent recovery on turbot *Scophthalmus maximus*: hormonal changes and anaerobic metabolism. *Mar. Ecol. Prog.* 225, 275–285. doi: 10.3354/meps225275

Pichavant, K., Person-Le-Ruyet, J., Le Bayon, N., Sévère, A., Le Roux, A., Quéméner, L., et al. (2000). Effects of hypoxia on growth and metabolism of juvenile turbot. *Aquaculture* 188, 103–114. doi: 10.1016/S0044-8486(00)00316-1

Qiao, H., Hu, D., Ma, J., Wang, X., Wu, H., and Wang, J. (2019). Feeding effects of the microalga Nannochloropsis sp. on juvenile turbot (*Scophthalmus maximus L.*). *Algal Res.* 41, 101540. doi: 10.1016/j.algal.2019.101540

Rector, M. E., Weitzman, J., Filgueira, R., and Grant, J. (2022). Environmental indicators in salmon aquaculture research: A systematic review. *Rev. Aquacult.* 14, 156–177. doi: 10.1111/raq.12590

Sanahuja, I., Ruiz, A., Firmino, J. P., Reyes-López, F. E., Ortiz-Delgado, J. B., Vallejos-Vidal, E., et al. (2023). *Debaryomyces hansenii* supplementation in low fish meal diets promotes growth, modulates microbiota and enhances intestinal condition in juvenile marine fish. *J. Anim. Sci. Biotechnol.* 14, 90. doi: 10.1186/s40104-023-00895-4

Schurch, N. J., Cole, C., Sherstnev, A., Song, J., Duc, C., Storey, K. G., et al. (2014). Improved annotation of 3′ Untranslated regions and complex loci by combination of strand-specific direct RNA sequencing, RNA-seq and ESTs. *PloS One* 9, e94270. doi: 10.1371/journal.pone.0094270

Schurch, N. J., Schofield, P., Gierliński, M., Cole, C., Sherstnev, A., Singh, V., et al. (2016). How many biological replicates are needed in an RNA-seq experiment and which differential expression tool should you use? *RNA* 22, 839–851. doi: 10.1261/rna.053959.115

Song, Z., Ye, W., Tao, Y., Zheng, T., Qiang, J., Li, Y., et al. (2023). Transcriptome and 16S rRNA analyses reveal that hypoxic stress affects the antioxidant capacity of largemouth bass (*Micropterus salmoides*), Resulting in Intestinal Tissue Damage and Structural Changes in Microflora. *Antioxidants* 12, 1. doi: 10.3390/antiox12010001

Soyluoglu, M., Kim, D., Zaker, Y., and Karanfil, T. (2021). Stability of oxygen nanobubbles under freshwater conditions. *Water Res.* 206, 117749. doi: 10.1016/j.watres.2021.117749

Tamber, S. S., Bansal, P., Sharma, S., Singh, R. B., and Sharma, R. (2023). Biomarkers of liver diseases. *Mol. Biol. Rep.* 50, 7815–7823. doi: 10.1007/s11033-023-08666-0

Tan, C., Zhao, W., Wen, W., Chen, X., Ma, Z., and Yu, G. (2022). Unraveling the effects of sulfamethoxazole on the composition of gut microbiota and immune responses in *Stichopus variegatus*. *Front. Microbiol.* 13. doi: 10.3389/fmicb.2022.1032873

Thu Lan, N. G., Dong, H. T., Vinh, N. T., Salin, K. R., Senapin, S., Pimsannil, K., et al. (2024). A novel vaccination strategy against *Vibrio harveyi* infection in Asian seabass (*Lates calcarifer*) with the aid of oxygen nanobubbles and chitosan. *Fish Shellfish Immunol.* 149, 109557. doi: 10.1016/j.fsi.2024.109557

Vacca, I. (2017). The microbiota maintains oxygen balance in the gut. *Nat. Rev. Microbiol.* 15, 574–575. doi: 10.1038/nrmicro.2017.112

Wang, Q. (2022). Effects of environmental stress (thermal, hypoxia) onthe ferroptosis pathway of turbot and its molecular mechanism. (Thesis). *Chin. Acad. Agric. Sci.* doi: 10.27630/d.cnki.gznky.2022.000896

Wang, Y., Peng, Z., Yan, L., Gao, X., Wu, L., Cui, S., et al. (2024). Effects of dietary glutamine supplementation on growth performance, intestinal digestive ability, antioxidant status and hepatic lipid accumulation in *Xenocypris davidi* (Bleeker,1871). *Aquacult. Int.* 32, 725–743. doi: 10.1007/s10499-023-01187-4

Wang, Z., Pu, D., Zheng, J., Li, P., Lü, H., Wei, X., et al. (2023). Hypoxia-induced physiological responses in fish: From organism to tissue to molecular levels. *Ecotoxicol. Environ. Saf.* 267, 115609. doi: 10.1016/j.ecoenv.2023.115609

Wang, J., Shi, Y., Elzo, M. A., Dang, S., Jia, X., and Lai, S. (2018). Genetic diversity of *ATP8* and *ATP6* genes is associated with high-altitude adaptation in yak. *Mitochondrial. DNA Part A.* 29, 385–393. doi: 10.1080/24701394.2017.1285292

Wang, H., Xia, B., Lin, M., Wang, Y., Sun, B., and Li, Y. (2020). Succinic acid inhibits the activity of cytochrome P450 (CYP450) enzymes. *Pharm. Biol.* 58, 1159–1164. doi: 10.1080/13880209.2020.1839110

Wu, S., Huang, J., Li, Y., and Pan, Y. (2023). Dynamic and systemic regulatory mechanisms in rainbow trout (*Oncorhynchus mykiss*) in response to acute hypoxia and reoxygenation stress. *Aquaculture* 572, 739540. doi: 10.1016/j.aquaculture.2023.739540

Wu, L., Li, J., Liu, F., Song, Z., Song, C., Xu, S., et al. (2024). Comparative transcriptome analyses reveal changes of gene expression in turbot (*Scophthalmus maximus*) embryos exposed to different LED light spectra and potential photosensitive function of non-visual opsins. *Aquacult. Rep.* 35, 101948. doi: 10.1016/j.aqrep.2024.101948

Wu, X., Li, D., Lu, J., Liu, L., Yang, Q., Tang, R., et al. (2023). Adaptation strategies of juvenile grass carp (*Ctenopharyngodon idella*) facing different dissolved oxygen

concentrations in a recirculating aquaculture system. *Water Biol. Secur.* 2, 100202. doi: 10.1016/j.watbs.2023.100202

Wu, Z., You, F., Wen, A., Ma, D., and Zhang, P. (2016). Physiological and morphological effects of severe hypoxia, hypoxia and hyperoxia in juvenile turbot (*Scophthalmus maximus L.*). *Aquacult. Res.* 47, 219–227. doi: 10.1111/are.12483

Xie, L., Tao, Y., Shen, Z., Deng, H., Duan, X., Xue, Y., et al. (2024). Congenital asplenia impairs heme-iron recycling during erythropoiesis in zebrafish. *Dev. Comp. Immunol.* 151, 105108. doi: 10.1016/j.dci.2023.105108

Xu, Y., Li, L., Lou, S., Tian, J., Sun, S., Li, X., et al. (2022). Effects of nano-aerators on microbial communities and functions in the water, sediment, and shrimp intestine in *Litopenaeus vannamei* aquaculture ponds. *Microorganisms* 10, 1302. doi: 10.3390/microorganisms10071302

Yang, Y., Wang, Z., Wang, J., Lyu, F., Xu, K., and Mu, W. (2021). Histopathological, hematological, and biochemical changes in high-latitude fish *Phoxinus lagowskii* exposed to hypoxia. *Fish Physiol. Biochem.* 47, 919–938. doi: 10.1007/s10695-021-00947-4

Yaparatne, S., Morón-López, J., Bouchard, D., Garcia-Segura, S., and Apul, O. G. (2024). Nanobubble applications in aquaculture industry for improving harvest yield, wastewater treatment, and disease control. *Sci. Total Environ.* 931, 172687. doi: 10.1016/j.scitotenv.2024.172687

Zhang, R., Zhang, Y., Chen, Y., Zhang, Y., Guo, J., Zhao, X., et al. (2024). Effects of composite lactic acid bacteria on the growth, intestinal physiology, and non-specific immunity of sea cucumber (*Apostichopus japonicus*). *Aquacult. Int.* 33, 52. doi: 10.1007/s10499-024-01681-3

Zhou, Y., Bastida, F., Liu, Y., He, J., Chen, W., Wang, X., et al. (2022). Impacts and mechanisms of nanobubbles level in drip irrigation system on soil fertility, water use efficiency and crop production: The perspective of soil microbial community. *J. Clean. Prod.* 333, 130050. doi: 10.1016/j.jclepro.2021.130050

Glossary

RAS	recirculating aquaculture system
DO	dissolved oxygen
NB-O_2	oxygen nanobubble
OTU	operational taxonomic unit
DEGs	differentially expressed genes
IBL	initial body length
FBL	final body length
IBW	initial body weight
FBW	final body weight
VSI	visceral index
ISI	intestinal index
LVI	liver index
BWG	body weight gain
FCR	feed conversion rate
SR	survival rate
SGR	specific growth rate
RR	respiratory rate
CF	coefficient of fatness
ABC	ATP-binding cassette
PPAR	peroxisome proliferators-activated receptors
LOC5547	uncharacterized LOC118285547
TG1	thyroglobulin, transcript variant X1
IIP44	interferon-induced protein 44-like
EPOD	eosinophil peroxidase-like
GTP7	GTPase IMAP family member 7-like
MYH1s	myosin heavy chain, fast skeletal muscle, transcript variant X1
PA2LY6	phospholipase A2 inhibitor and Ly6_PLAUR domain-containing protein
Mucin5	mucin-5AC-like
FNDC7	fibronectin type III domain containing 7a
NOS1	nitric oxide synthase 1 (neuronal)
ATP6	ATP synthase F0 subunit 6
ATP8	ATP synthase F0 subunit 8
COX1	cytochrome c oxidase subunit I
HIF1	hypoxia inducible factor 1 subunit alpha, like, transcript variant X1
Hbae5	hemoglobin, alpha embryonic 5
Man-SL	mannose-specific lectin-like
HSP90	heat shock protein 90, beta (grp94), member 1
CYP450	cytochrome P450, family 1, subfamily B, polypeptide 1
β-actin	actin, beta 2
WBC	white blood cells
RBC	red blood cells
HGB	hemoglobin
TP	total protein
ALB	albumin
GLOB	globulin
HCT	hematocrit
MCV	mean corpuscular volume
PLT	platelets
C(tO_2e)	total oxygen content
S(O_2)	oxygen saturation
CHO	cholesterol
TG	triglycerides
GLU	glucose
BUN	blood urea nitrogen
CRE	creatinine
MDA	malondialdehyde
ACP	acid phosphatase
AKP	alkaline phosphatase
PPO	polyphenol oxidase
LZM	lysozyme
LDH	lactate dehydrogenase
SDH	succinate dehydrogenase
GPT	glutamic pyruvic transaminase
GOT	glutamic oxalacetic transaminase